Doctoral Dissertation

The Model of Continuous Conduction Mode and Mode Control in Power Converter

---

September, 2018

University of Miyazaki

Interdisciplinary Graduate School of Agriculture and Engineering

Department of Materials and Informatics

Eko Setiawan

Supervisor: Professor Ichijo Hodaka

Abstract

The power converter is one of the fundamental parts of any electronics system. The power converter provides a required voltage or current of the system. Failure on the design and control of power converter affects the main system defective. In order to design a power converter with the specification, the engineers should use a model that represents the system mathematically. A power converter has two modes which are called a continuous conduction mode (CCM) and a discontinuous conduction mode (DCM). Most researches design the system based on CCM, but they never guaranteed that their system would stay on CCM. If the system goes to DCM, but the system is designed in CCM, the converter may lapse into behavior out of specification.

In Chapter 2, this dissertation proposes to use a symbolic steady-state model of the buck converter. Since the steady-state response is a periodic signal with a period of switching, it may have a Fourier series representation. It is easy to calculate the Fourier series if we are given a numerically represented signal. However, it does not give a clear relationship between constants in the circuit elements and constants in the behavior such as an average and a ripple of voltages and currents. This dissertation will decompose the steady state signal of buck converter into a sum of several periodic functions called recovery functions. This process is done with a symbolic calculation and enables to know how a constant in the circuit elements affects a constant such as a ripple. The information about the effect of the constant would give a clear design step of the buck converter.

In Chapter 3, this dissertation proposes a nonlinear control of boost converter that forces the behavior inside the CCM region. The idea of the design step is to use a phase portrait of behavior. Since the controller is given with geometrically understood way, it could describe an initial condition and a reference condition on the portrait. The proposed controller is shown to bring the voltage and current to a reference point without going into DCM region. The simulation and experiment results show that the proposed controller successfully keeps the boost converter on CCM in some initial conditions.

In Chapter 4, this dissertation summarizes a control problem in the power converter and describes how the proposed ideas are used to the problem. Then it is

pointed out that their ideas may be applied to some problems in power conversion for the future works.

Keywords: *power converter, buck converter, boost converter, continuous conduction mode, Fourier series, steady state model, phase portrait, nonlinear mode control*

Acknowledgement

The study has done in Automatic Control System Laboratory, Interdisciplinary Graduate School of Agriculture and Engineering, University of Miyazaki, under the supervision of Prof. Ichijo Hodaka. The author would like to express his great gratitude to Prof. Ichijo Hodaka for all support and all guide that he provides throughout the author doctoral degree. The author also thanks Prof. Ichijo Hodaka for trusting the author in finishing the doctoral degree.

The high appreciation and thanks to the committee members: Prof. Hiroki Tamura, Prof. Koichi Tanno, Prof. Osamu Sato and Prof. Masahiro Tasumi, for their generous time in giving their thoughtful suggestions and constructive advice for the improvement of this dissertation.

The author would like to acknowledge the Ministry of Education, Culture, Sports, Science, and Technology (MEXT) of Japan for the scholarship during the doctoral degree.

The author thanks all laboratory members: Kazuya Yamaguchi, Takuya Hirata, Masahiro Ienaga, Shigefumi Morita, Masahiro Hayashi, Alfius Pagawak, Cheikh Fall, M. Afnan Habibi, Mayu Suzuki and the other laboratory members for their help, corporate and fun in laboratory life.

The author would like to give his heartfelt gratitude to his wife, Bunga Hidayati and his daughter, Camelia Akira Setiawan who gives support and spirit during this study. The author would like to express his great respect to his parents for many given wise advice in the author's life while completing the doctoral degree. The author would like to show thankfulness to his friends and communities for the support during living in Japan.

Above all, the author gives his spiritual grateful to the Almighty Allah SWT, for the opportunity, health and strength to accomplish this work.

Dedicated to beloved wife, Bunga Hidayati, lovely child, Camelia Akira Setiawan, and respected parents, Harjito and Mariyati

Contents

List of Figures

List of Tables

Chapter 1

General Introduction

1.1 Background

An electronic system requires a specific voltage to work correctly. On the other hand, the voltage source (such as a battery) does not always provide the required voltage. Here, a power converter is often used to adjust the voltage of the battery so that it fits with the voltage of the electronics system. The power converter position is between the voltage source and the electronic system. Since the power converter has a vital role in providing the required power, the design of power converter becomes a critical section in an electronics system.

A power converter usually works with a controller. The controller can keep the converter delivering a constant output voltage by adjusting the trigger signal of power converter automatically. The model of power converter should be known mathematically if we want to design the automatically control system. The model shows the relationship between the trigger signal to the output voltage of power converter. If the controller knows the relationship, it can estimate how large the trigger signal should be given to the converter. This fact explains that the model of power converter is absolutely required in the controller design.

The earlier technique designs the controller based on linear model approximation at a specific point. The illustration of technique is shown in Figure 1.1. This techniques is also known as *perturbation and linearization* [1]. Using this linearized model, the controller designer can adapt the numerous linear time-invariant (LTI) control theory to solve the problem in power converter. The solution may only work well on partial condition of power converter because the linearized model is only similar with the actual model on partial sections. The fact tells that a power converter is not an LTI system. It means that there is still no general solution for a power converter control problem.

This dissertation focuses on modeling of power converter and the controller

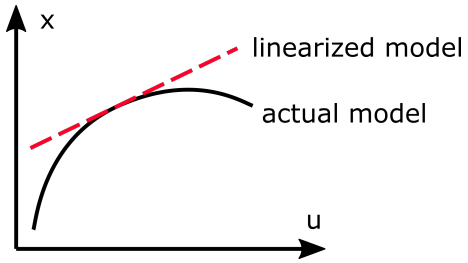

Figure 1.1: Linearization of the model

design. This dissertation observes two topologies of power converter which are buck converter and boost converter. The buck converter has different characteristic with boost converter. The different approximation is utilized to solve the problem on each converter. A novel techniques in modeling and control design is presented in this dissertation.

1.2 Objectives

The objectives of this dissertation is to provide a solution of control problem for power converter including the modeling technique. The solution should consider the correctness of converter model which is used to solve the problem. It is true that some assumptions can simplify the model but it may cut some information. This dissertation considers the missing information. Moreover, the consistency between model, controller and system behavior should be kept carefully so the solution is guaranteed always correct. This dissertation keeps the consistency of continuous conduction mode (CCM) model while it solves the power converter control problem.

1.3 Fundamental Theories

Some fundamental theories are useful before reading this dissertation further. The theories bring the same perception between the author and readers. This section will explain some theories in several subsections.

1.3.1 Power Converters

The power converter is also known as a DC-DC converter in reference [2]. The origin of the DC-DC converter term comes from its direct current (DC) input voltage and its DC output voltage. The term explains that the circuit converts a DC input voltage into a desired DC output voltage. The other references [1, 3] also called it as switching converter due to its principle work. The converter works

by switching from one state to another state in the high speed. Some electronics parts such as metal oxide semiconductor field effect transistor (MOSFET) which is controlled by a trigger signal do this switching mechanism. By this switching mechanism, the converter can increase or decrease the output voltage depended on the duration of one state to the other state.

There are some topologies of power converters such as buck converter, a boost converter, a buck-boost converter, or SEPIC. Each topology has a specific characteristic. The end of this subsection summarizes the characteristic of some converters. Figure 1.2 shows several topologies of the DC-DC converter. Principally, the power converter works by connecting each switch (SW) to the node-1 or node-2 alternately.

Buck Converter

The explanation starts with the principal of the buck converter. The analysis will be similar for the others topologies of the power converter. A buck converter can only decrease the output voltage to its input voltage. The duration when the switch SW (shown in Figure 1.2) connects the node-1 or node-2, adjusts the voltage decrement level. The explanation of buck converter characteristic is obtained by its steady state analysis which is derived by using the principle of *inductor volt-second balance* and *capacitor charge balance* [1]. The inductor volt-second balance means that the average voltage of an inductor will be equal to zero on the steady state in one period. The capacitor charge balance means the current of the capacitor will be zero on the steady state in one period. The capacitor will stay at a certain voltage, and there is no significant change in inductor current. The following equations describe the mathematical expression of inductor volt-second balance and capacitor charge balance.

$$\bar{v_L} = \frac{1}{T_s}\int_0^{T_s} v_L(t)dt = 0 \tag{1.1}$$

$$\bar{i_C} = \frac{1}{T_s}\int_0^{T_s} i_C(t)dt = 0 \tag{1.2}$$

where

$$\begin{aligned} \bar{v_L} &= \text{average inductor voltage} \\ v_L(t) &= \text{voltage of inductor on } t \\ \bar{i_C} &= \text{average capacitor current} \\ i_C(t) &= \text{current of capacitor on } t \\ T_s &= \text{switching time-period} \end{aligned}$$

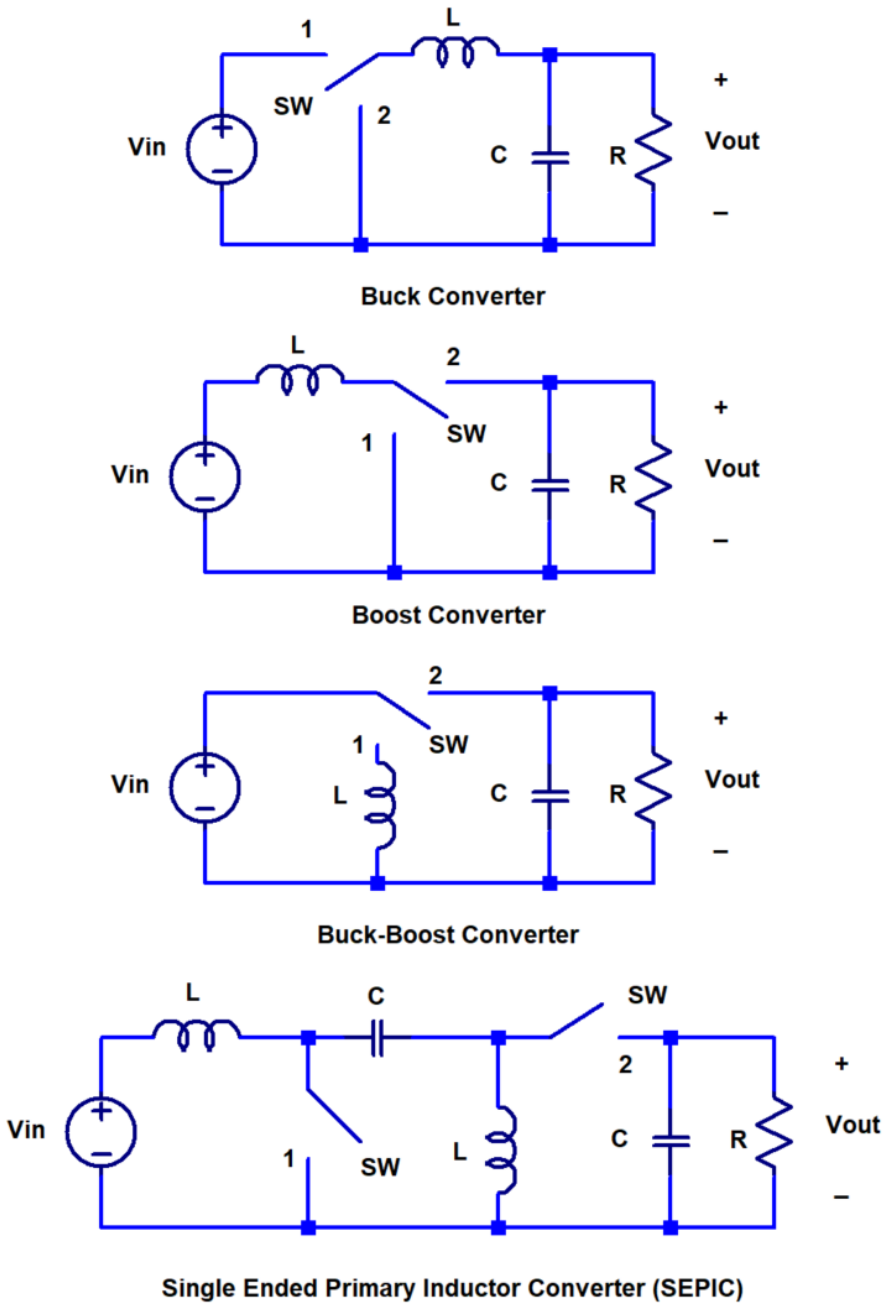

Figure 1.2: Various kinds of power converter

This paragraph derives the equation of buck converter. As described beforehand, the switch SW connects to the node-1 or the node-2 alternatively. The analysis begins with the switch SW connected to node-1. This state is *mode-1* in this chapter. Figure 1.3 shows the buck converter in mode-1. The Kirchoff Voltage and Current Law (KVL and KCL) of the converter are in the following equation.

$$\begin{aligned} v_L(t) &= V_{in} - V_{out} \\ i_C(t) &= i_L(t) - \frac{V_{out}}{R} \end{aligned} \tag{1.3}$$

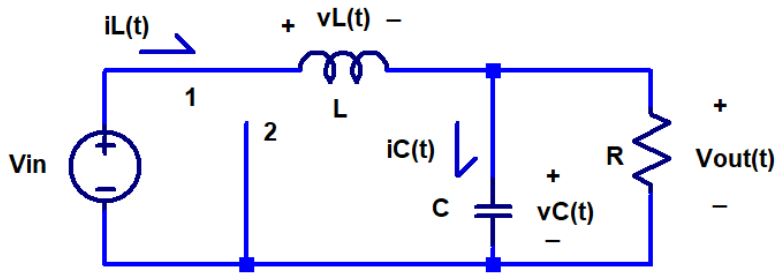

Figure 1.3: Buck converter on mode-1

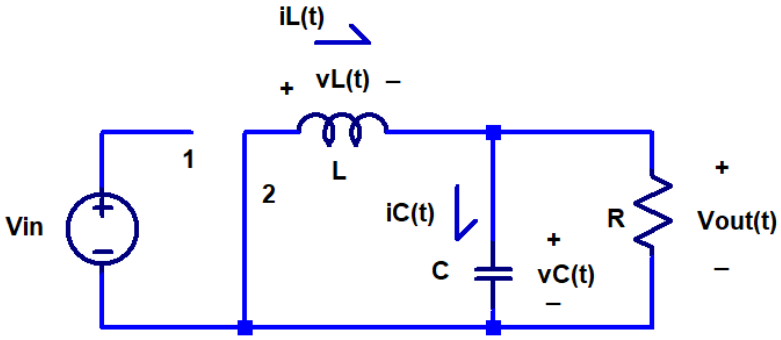

Figure 1.4: Buck converter on mode-2

The other state of buck converter occurs when the switch SW connected to the node-2, called as *mode-2*. The circuit can be simplified as shown in Figure 1.4. The following equation shows the equation of Figure 1.4.

$$\begin{aligned} v_L(t) &= -V_{out} \\ i_C(t) &= i_L(t) - \frac{V_{out}}{R} \end{aligned} \tag{1.4}$$

Then, the equation (1.1) and (1.2) derive the steady-state characteristic of the buck converter. We assume that the mode-1 is occurred from $t = 0$ until $t < DT_s$ and the mode-2 occurs when $DT_s \leq t < T_s$. The variable T_s is the switching period of the power converter. Then, the equation (1.3) and (1.4) complete the

integration of equation (1.1) as follows.

$$\begin{aligned}
\bar{v_L} &= \frac{1}{T_s}\left(\int_0^{DT_s} v_L(t)dt + \int_{DT_s}^{T_s} v_L(t)dt\right) \\
&= \frac{1}{T_s}\left(\int_0^{DT_s} (V_{in} - V_{out})dt + \int_{DT_s}^{T_s} (-V_{out})dt\right) \\
&= \frac{1}{T_s}\left((V_{in} - V_{out})\, DT_s - V_{out})(1-D)T_s\right) \\
0 &= V_{in}D - V_{out} \\
V_{out} &= DV_{in}, \qquad (1.5)
\end{aligned}$$

where D = ratio of the period.

Based on (1.5), the change of D adjusts the output voltage. The D is a limit of the switch SW connected to node-1 or node-2. Most power converter uses a metal-oxide-semiconductor field effect transistor (MOSFET) as an electronics switch. Then, the DT_s is a trigger signal duration that makes the MOSFET of $SW-1$ conducts or it is a trigger signal that turns off the MOSFET in $SW-2$. By changing the ratio D, we can adjust the converter output voltage. The pulse width modulation (PWM) signal to the gate of MOSFET realizes the switching mechanism of the converter. The subsection 1.3.2 explains the hardware implementation of the power converter in detail.

The steady state of the other power converters

The others converters also can be derived by a similar technique as explained in a buck converter. The following equations summarize the steady-state characteristics of the other converters.

$$\begin{aligned}
&\text{Buck converter :} && V_{out} = DV_{in} \\
&\text{Boost converter :} && V_{out} = \frac{1}{1-D}V_{in} \\
&\text{Buck-boost converter :} && V_{out} = \frac{-D}{1-D}V_{in} \\
&\text{SEPIC :} && V_{out} = \frac{D}{1-D}V_{in} \qquad (1.6)
\end{aligned}$$

where $0 \leq D \leq 1$. The summarized characteristic shows that the buck converter only produces the output voltage less than or equal with its input voltage. The boost converter only can increase the output voltage to its input voltage. The buck-boost converter and SEPIC can deliver the less or greater output voltage than its input voltage. The output voltage of the buck-boost converter and SEPIC have different in voltage polarity. This information is essential in selection converter

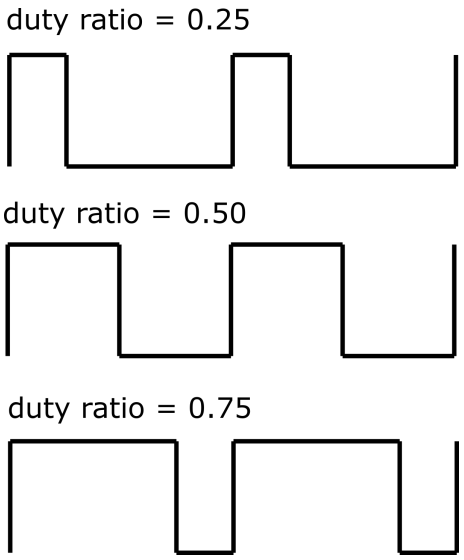

Figure 1.5: Pulse width modulation

topology which should be used based on system needs.

1.3.2 Pulse Width Modulation in Power Converter

The knowledge of pulse width modulation (PWM) is fundamental to understand how the power converter works. A PWM signal is a square-wave signal with a constant periodic. A PWM signal modulates information by changing the ratio between high signal and low signal as shown in Figure 1.5. The ratio of high signal and a low signal is known as duty ratio (D) of the PWM signal. The boundary of the duty ratio is from 0 to 1.

The PWM signal can control the output power converter by connecting it to the gate pin of the metal-oxide-semiconductor field effect transistor (MOSFET). A MOSFET can work as a switch in an electronics system. A MOSFET has a gate pin which controls the behavior of MOSFET. The n-type MOSFET can conduct the current when a high voltage is connected to its gate pin. The n-type MOSFET can cut-off the current when its gate pin has a zero voltage. Different type of MOSFET may have reversed behavior. The specific references about MOSFET show the further information about MOSFET characteristic. The converter uses MOSFET and diode to realize the switch. Figure 1.6 shows the circuit realization of the power converter. Figure 1.6 uses n-type MOSFET as a switch. The MOSFET will conduct the current if the PWM voltage is a high signal. The MOSFET will be disconnected if the PWM is low signal and the diode will conduct as replacement of SW and node-2 in Figure 1.2.

On the equation (1.6), variable D which is the ratio of the period adjusts the output voltage. The D decides the state of switch SW. By using PWM and MOS-

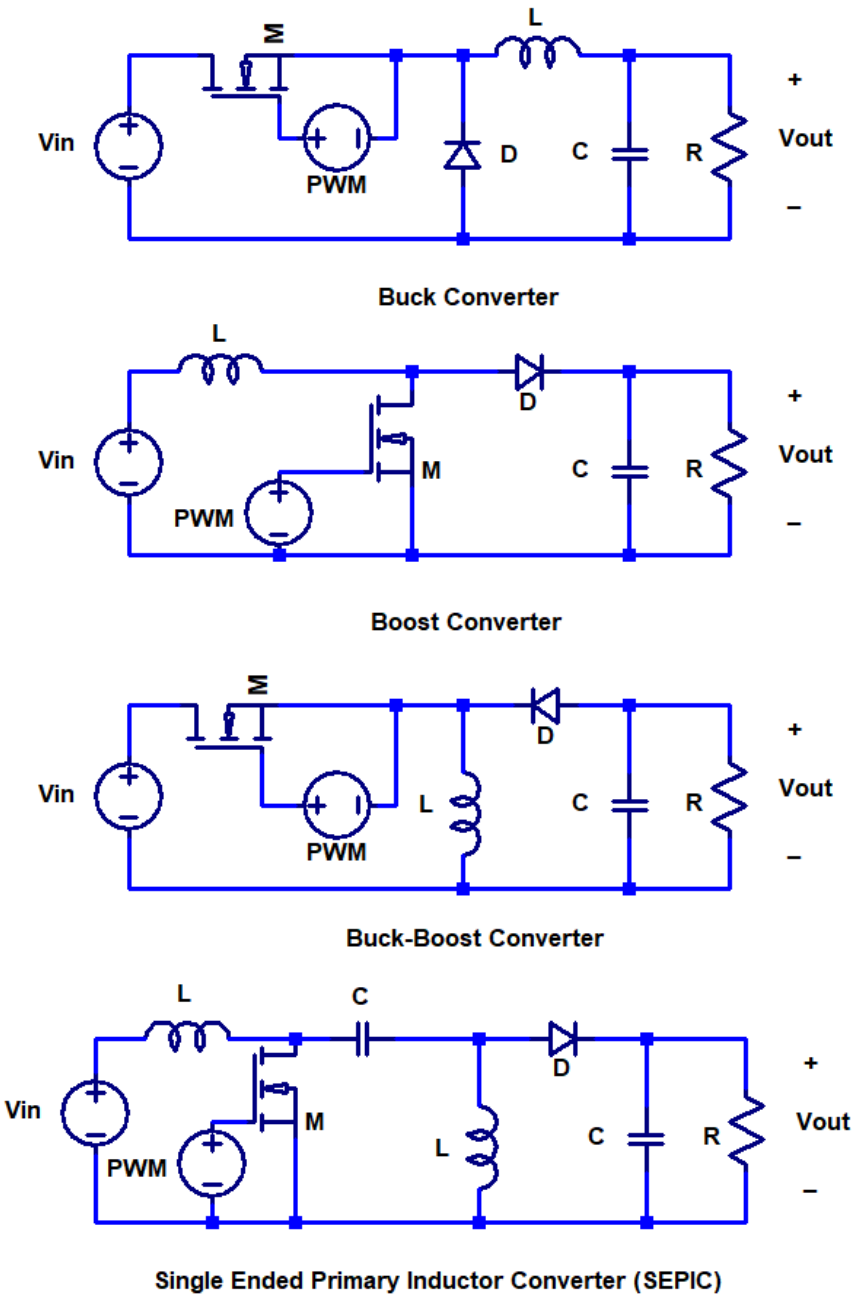

Figure 1.6: Various kind of power converter in the circuit implementation

FET, the ratio of period D will be equal to the behavior of the PWM duty ratio to the MOSFET as a switch. We can control the output voltage by changing the duty ratio of PWM.

Besides using diodes and MOSFET, both switches can use MOSFET entirely as shown in Figure 1.7 of the buck converter. The contrary PWM is required to switch both MOSFET alternately. This topology is known as a synchronous power converter. The synchronous power converter has an advantage in the flexibility of converter modes adjustment.

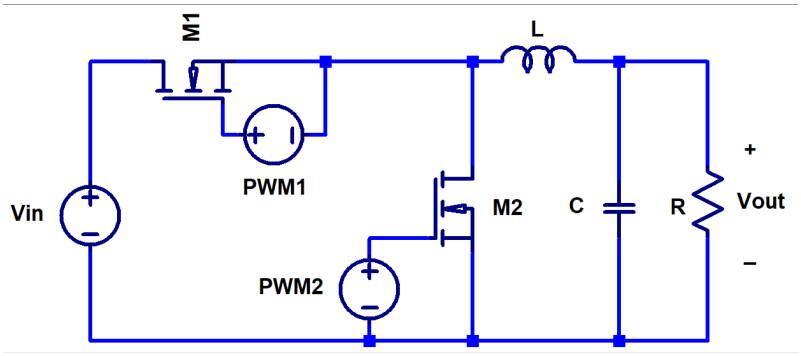

Figure 1.7: A synchronous buck converter

1.3.3 Continuous and Discontinuous Conduction Mode

In the standard condition, the power converter works by switching from one mode or state to the other alternately as explained in subsection 1.3.1. This switching occurs continuously during a life cycle of the power converter. This conduction is known as Continuous Conduction Mode (CCM). The CCM means that the converter only has two states per switching cycle.

When the switches of the power converter are implemented using current uni-directional or voltage uni-directional semiconductor switches, one new mode of operation known as Discontinuous Conduction Mode (DCM) can occur. The discontinuous conduction mode arises when the switching ripple in an inductor current or capacitor voltage is large enough to cause the polarity of the applied switch current or voltage to reverse [1].

In order to give a straightforward description, this subsection will give an illustration about the inductor current or capacitor voltage of buck converter. This subsection explains the buck converter only, but the other type of converter can use the similar technique as explained in this subsection. Figure 1.6 shows the topology of the buck converter. The buck converter consists of the diode which is the uni-directional current semiconductor switch. It means the DCM can occur during the converter life cycle

Figure 1.8 illustrates the output voltage of the buck converter. Based on Figure 1.8, the output voltage is not constant. The voltage ripple illustrated in triangle waveform. This waveform comes from switching mechanism. Based on Figure 1.3, the circuit charges the capacitor during mode-1. This condition causes the capacitor voltage or output voltage increases in mode-1. For the mode-2 in Figure 1.4, the capacitor will be discharged to supply the load due to the disconnected input voltage source. This condition makes the output voltage decrease as shown in Figure 1.8. The switching frequency does not change the average output voltage ($\bar{v}_{out}$). The frequency affects the output voltage ripple which illustrated in the

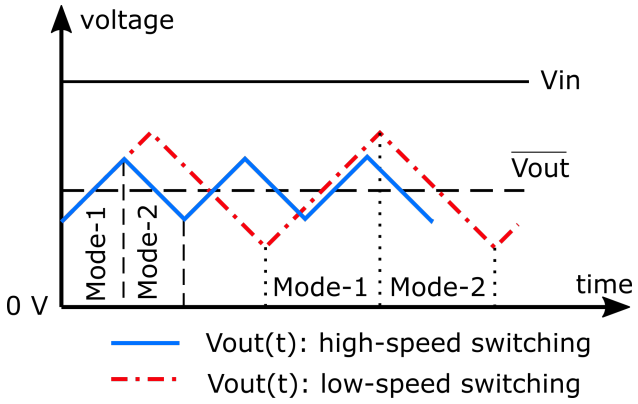

Figure 1.8: Capacitor voltage of the buck converter

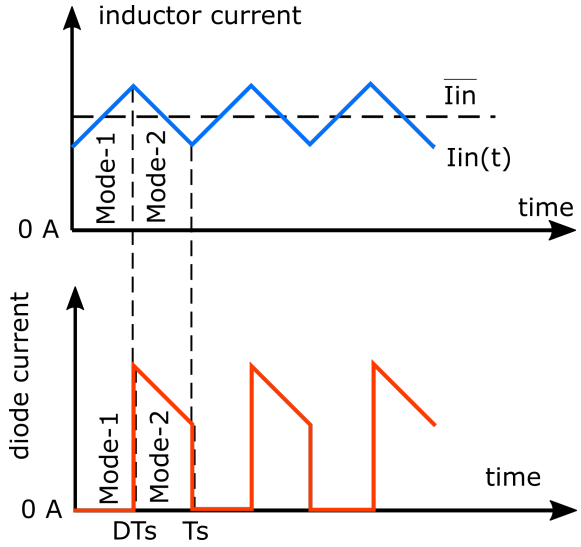

Figure 1.9: Current of buck converter in CCM

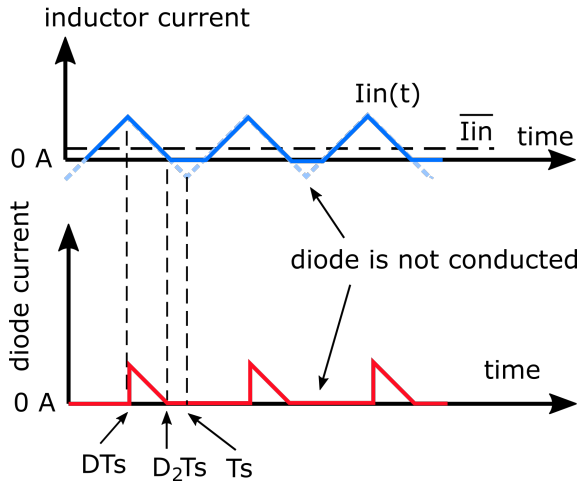

Figure 1.10: Current of a buck converter in DCM

triangle waveform. The low-speed switching or extended period creates the high amplitude ripple.

The phenomenon of ripple also occurs to the inductor current. The inductor

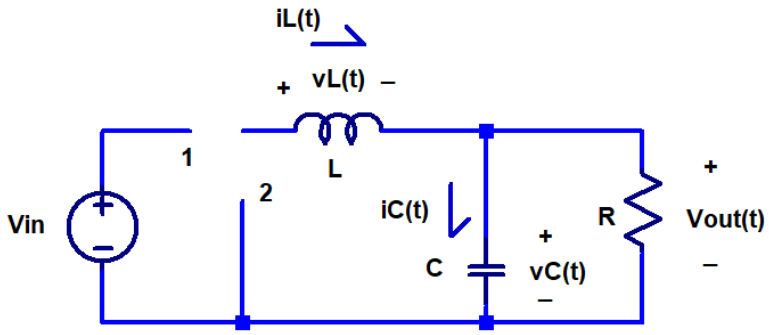

Figure 1.11: An additional mode in DCM of the buck converter

current also consists of the ripple as illustrated in Figure 1.9. Figure 1.4 shows the simple topology of mode-2 clearly. Since the diode is only active on the mode-2 and the diode current is equal to the inductor current, the diode current curve only has value on mode-2. Although the switching frequency is constant, the inductor current may change depending on load and given duty ratio. The discontinuous of conduction occurs when the inductor current approaches to zero as shown in Figure 1.10. Since the diode is a uni-directional current semiconductor device, the negative current cannot through the diode. This condition means both switches (MOSFET and diode) are disconnected. The switches are inactive at a particular time ($D_2T_s - T_s$) as shown in Figure 1.11. As a consequence, the steady-state characteristic of the buck converter will change as shown in the following equation.

$$\begin{aligned} V_L &= \frac{1}{T_s}\left(\int_0^{DT_s}(V_{in}-V_{out})dt + \int_{DT_s}^{D_2T_s}(-V_{out})dt + \int_{D_2T_s}^{T_s}0dt\right) \\ &= \frac{1}{T_s}\left((V_{in}-V_{out})\,DT_s - V_{out})(D_2-D)T_s\right) \\ 0 &= V_{in}D - V_{out}D_2 \\ V_{out} &= \frac{D}{D_2}V_{in} \end{aligned} \tag{1.7}$$

The DCM analysis needs the knowledge about time constant D_2. This value is uncertain and depends on the component parameter of the converter. Since the DCM is more complicated than CCM, most of the researches analyze the converter only on CCM.

1.3.4 State Space Representation

The state space equation is according to the knowledge of a set of n first-order differential equation involving so-called state variables, which denoted as $x_1(t)$, $x_2(t)$, ..., $x_n(t)$ [4]. The state space allows us to analyze all variable in a matrix repre-

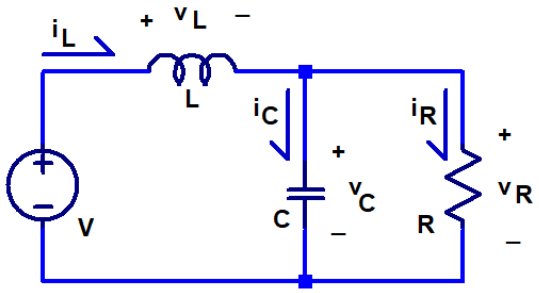

Figure 1.12: RLC circuit

sentation. In order to understand the state space representation, the explanation starts from the equations of the circuit in Figure 1.12. The circuit consists of an inductor L, a capacitor C, a resistor R and a voltage source V. The characteristic of each component is described in the following equations.

$$\begin{aligned} v_R &= i_R R \\ v_L &= L\frac{di_L}{dt} \\ i_C &= C\frac{dv_C}{dt} \end{aligned} \tag{1.8}$$

Where v_R is the voltage of resistor, i_R is the current of resistor and so on. Using a Kirchhoff Voltage and Current Law, the equation of the circuit is derived as follows.

$$\begin{aligned} V &= v_L + v_C \\ &= L\frac{di_L}{dt} + v_C \\ \frac{di_L}{dt} &= \frac{V}{L} - \frac{v_C}{L} \end{aligned} \tag{1.9}$$

$$\begin{aligned} i_L &= i_C + i_R \\ &= C\frac{dv_C}{dt} + \frac{v_C}{R} \\ \frac{dv_C}{dt} &= \frac{i_L}{C} - \frac{v_C}{RC} \end{aligned} \tag{1.10}$$

If we want to find the solution of i_L or v_C, we cannot solve it separately. It because the inductor current is affected by the capacitor voltage and vice verse. The two ordinary differential equation (ODE) (1.9) and (1.10) can be represented in the single linear algebra of ordinary differential equation. The matrix represen-

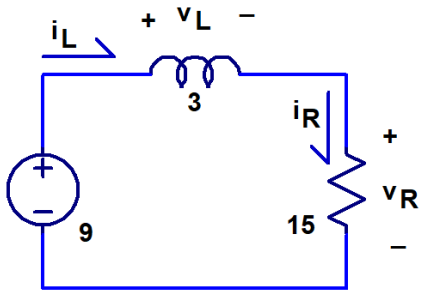

Figure 1.13: RL circuit

tation of Figure 1.12 is as follows.

$$\frac{d}{dt}\begin{bmatrix} i_L \\ v_C \end{bmatrix} = \begin{bmatrix} 0 & \frac{-1}{L} \\ \frac{1}{C} & \frac{-1}{RC} \end{bmatrix}\begin{bmatrix} i_L \\ v_C \end{bmatrix} + \begin{bmatrix} \frac{V}{L} \\ 0 \end{bmatrix} \tag{1.11}$$

The equation (1.11) is a state space representation of the circuit. As the consequence of state space, we can solve the equation simultaneously. The following equation express the state space equation in a general form.

$$\dot{x} = Ax + b \tag{1.12}$$

where

$$x = \begin{bmatrix} x_1 \\ x_2 \\ \dots \\ x_n \end{bmatrix}$$

1.3.5 General Solution of State Space

The state space representation of the circuit has an advantage that it is possible to solve the equation simultaneously. The state space equation form is similar with a single first-order ordinary differential equation (ODE). Thus, the solution of the first-order ODE should work for the state space equation.

The discussion starts with the solution of the first-order ODE before finding the general solution of the state space equation. The solution of RL circuit shown in

Figure 1.13 is analyzed step-by-step. The following equations work for the circuit.

$$\begin{aligned} v_L &= V - v_R \\ \frac{di_L}{dt} &= \frac{-R}{L} i_L + \frac{V}{L} \\ \dot{i_L} &= -5i_L + 3 \end{aligned} \tag{1.13}$$

The solution of the ODE can be found by following steps.

$$\begin{aligned} \frac{di_L}{-5i_L + 3} &= dt \\ \int \frac{di_L}{-5i_L + 3} &= \int dt \\ \frac{-1}{5} \log\left(-5i_L + 3\right) &= t + C_1 \\ -5i_L + 3 &= e^{-5t-5C_1} \\ i_L &= \frac{-1}{5} e^{-5t-5C_1} + \frac{3}{5} \\ i_L(t) &= \underbrace{\frac{-1}{5} e^{-5C_1}}_{C} e^{-5t} + \frac{3}{5} \end{aligned} \tag{1.14}$$

An initial value of i_L is given in $i_L(0) = i_0$. Then, the constant C can be defined as follows.

$$\begin{aligned} i_L(0) &= Ce^{-5(0)} + \frac{3}{5} \\ i_0 &= C + \frac{3}{5} \\ C &= i_0 - \frac{3}{5} \end{aligned} \tag{1.15}$$

The equation (1.15) is substituted into (1.14). The solution of ODE becomes as follows.

$$\begin{aligned} i_L &= \left(i_0 - \frac{3}{5}\right) e^{-5t} + \frac{3}{5} \\ &= i_0 e^{-5t} - \frac{3}{5} e^{-5t} + \frac{3}{5} \end{aligned} \tag{1.16}$$

The last two parts of right-hand-side equation can be represented in the integral form as follows.

$$\begin{aligned} i_L &= i_0 e^{-5t} - \frac{3}{5} e^{-5t} + \frac{3}{5} \\ &= i_0 e^{-5t} + \int_0^t 3e^{-5(t-\tau)} d\tau \end{aligned} \tag{1.17}$$

The equation (1.17) is general solution for the first order ODE in the equation (1.13). If we take a look the equation (1.13) and (1.12), both of equation has similar structure. The state x in the equation (1.12) is similar with the variable i_L in the example of ODE (1.13). Then, the solution of state space equation in general form is described as follows.

$$\begin{aligned} \dot{x} &= Ax + b \\ x &= e^{At}x_{t0} + \int_{t0}^{t} e^{A(t-\tau)}bd\tau \end{aligned} \tag{1.18}$$

1.3.6 Exponential Matrix

The state space equation has an advantage in providing the solution of state variable simultaneously. Even the general solution of state space has already described in the previous subsection; another problem appears in the solution. In the first order ODE, the exponential appears in the solution. For the state space equation, the exponential is in the matrix form which is e^A. The exponential of a matrix has a proper calculation. This subsection explains how to calculate the exponential of a matrix.

This subsection introduces the diagonalization technique for a square matrix at the beginning. By applying the eigenvalues λ_i and eigenvectors v_i, it can write the matrix equality as follows.

$$\begin{aligned} A\,V &= V\,\Lambda \\ A\,[v_1|v_2...v_k] &= [v_1|v_2...v_k] \begin{bmatrix} \lambda_1 & 0 & ... & 0 \\ 0 & \lambda_2 & ... & 0 \\ ... & & & ... \\ 0 & 0 & ... & \lambda_k \end{bmatrix} \\ [Av_1 \mid Av_2...Av_k] &= [\lambda_1 v_1 \mid \lambda_2 v_2...\lambda_k v_k] \end{aligned} \tag{1.19}$$

Based on the fact, the matrix A is also can be represented in eigenvalues diagonal matrix as follows.

$$A = V\Lambda V^{-1} \tag{1.20}$$

An exponential function is defined in a series as follows.

$$e^{at} = 1 + at + \frac{(at)^2}{2!} + \frac{(at)^3}{3!} + ... + \frac{(at)^n}{n!} \tag{1.21}$$

which n is infinity to get the accurate approximation. The representation of expo-

nential in matrix also has similar form as follow.

$$e^{At} = I + At + \frac{A^2t^2}{2!} + \frac{A^3t^3}{3!} + ... + \frac{A^nt^n}{n!} \tag{1.22}$$

We can replace the matrix A with its diagonal form in (1.20) as follows.

$$\begin{aligned} A^2 &= V\Lambda V^{-1}.V\Lambda V^{-1} &&= V\Lambda^2 V^{-1} \\ A^3 &= V\Lambda V^{-1}.V\Lambda V^{-1}.V\Lambda V^{-1} &&= V\Lambda^3 V^{-1} \end{aligned} \tag{1.23}$$

Then, the exponential of matrix is rewritten as follows.

$$\begin{aligned} e^{At} &= VIV^{-1} + V\Lambda V^{-1}t + \frac{V\Lambda^2V^{-1}t^2}{2!} + \frac{V\Lambda^3V^{-1}t^3}{3!} + ... + \frac{V\Lambda^nV^{-1}t^n}{n!} \\ &= V\left[I + \Lambda t + \frac{\Lambda^2t^2}{2!} + ... + \frac{\Lambda^nt^n}{n!}\right]V^{-1} \end{aligned} \tag{1.24}$$

The inside of bracket can be calculated. Since Λ is a diagonal matrix, we only need to consider the diagonal position and put a zero number to the others.

$$= V\begin{bmatrix} 1+\lambda_1 t + \frac{\lambda_1^2t^2}{2!} + ... & 0 & ... & 0 \\ 0 & 1+\lambda_2 t + \frac{\lambda_2^2t^2}{2!} + ... & & 0 \\ ... & & & ... \\ 0 & 0 & ... & 1+\lambda_k t + \frac{\lambda_k^nt^n}{n!} + ... \end{bmatrix}V^{-1} \tag{1.25}$$

Rather than calculating its diagonal part, it is better to bring it back to the exponential form as follows.

$$e^{At} = V\begin{bmatrix} e^{\lambda_1 t} & 0 & ... & 0 \\ 0 & e^{\lambda_2 t} & ... & 0 \\ ... & & & ... \\ 0 & 0 & ... & e^{\lambda_k t} \end{bmatrix}V^{-1} \tag{1.26}$$

Based on the equation (1.26), finding the eigensystem beforehand can solve the exponential matrix. The equation (1.26) can be used to obtain the solution of state space equation in the equation (1.18).

1.4 Outline

This dissertation has four chapters. Figure 1.14 shows the connection between each chapter. **Chapter 1** gives a general introduction to this dissertation. The power converter control problem is described step-by-step in this chapter. This

chapter explains the objective of the study. Furthermore, there are the fundamental theories which are related to this dissertation in this chapter. The outline described in this chapter helps the reader to understand the story of this dissertation easily. The next chapters are the main content of this dissertation which had been in the articles [5, 6].

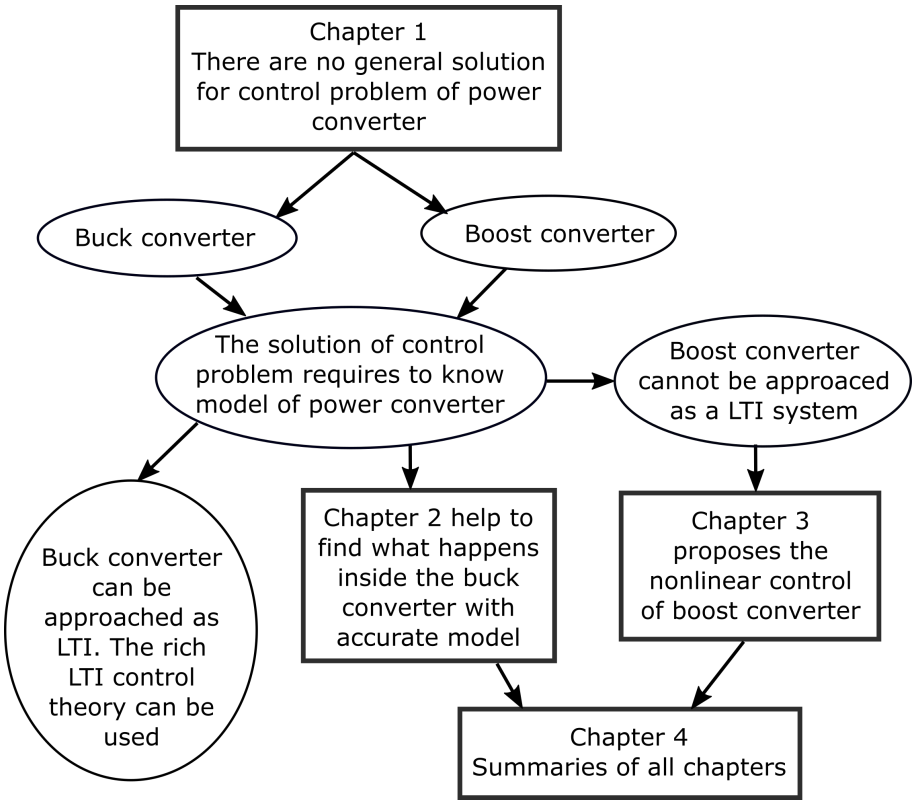

Figure 1.14: The outline of dissertation

There is the various topology of the power converter. This dissertation studies the buck converter and the boost converter. The buck converter is approachable in linear time-invariant (LTI) system which has numerous solution of control problem by averaging the input of buck converter. Since the modeling uses the averaging technique, we cannot know what exactly happens inside the converter. **Chapter 2** proposes the model to identify the behavior of the buck converter accurately in the steady state. Since the steady state is a periodic signal with a period of switching, it may have a Fourier series representation. This chapter decomposes the steady state signal of buck converter into a sum of several periodic functions called recovery function. The numerical circuit simulation affirms the proposed steady-state model.

Chapter 3 discusses the control problem solution on a boost converter. The boost converter is not similar to an LTI system. This chapter generates the model of the boost converter. Since the model is in two state variables, the behavior of converter can be examined using a two-dimensional plane called phase plane.

This chapter proposes a novel nonlinear control which comes from the manipulation of flow in the phase plane. The simulation is conducted to compare the proposed controller. Moreover, an experiment is done to show the controller is implementable.

Finally, the essence of each chapter is in **Chapter 4**. This chapter gives a summary of all study which compiles this dissertation. Moreover, future work is also in this chapter. The author realizes the time limitation of this study. Through a given future work, the study will be more useful in the engineering problem.

Chapter 2

An Accurate Symbolic Steady State Modeling of Buck Converter

2.1 Background

Most of the control system uses an averaging technique to construct the model of power converter [7–11]. The averaging copes the difficulty in converter modeling. This technique brings one advantage on a buck converter because we can approximate a converter into a linear time-invariant (LTI) system without linearization as shown in Figure 1.1. It makes the solution of an LTI system works perfectly for a buck converter.

However, the averaging techniques have a shortage in describing what happens inside the buck converter. The technique will cut the detailed behavior of buck converter and take the average of it. The model cannot show how big the ripple of the buck converter is and which parameter should be modified if we want to reduce it. The calculation of root-mean-square (RMS) is also impossible to do if we do not know the detail equation of the buck converter. The power electronic handbook approximate linear ripple to analyze DC-DC converter more accurately [1]. The approximation may be correct if the switching frequency is high. Since there is some limitation in the component, the switching frequency cannot always be high.

The importance of accurate steady-state analysis has already noticed in many types of research [12–17]. A significant part of the design of circuits requires the simulation of the steady-state response which shows some parameters such as the gain, harmonic distortion, the input and output impedances [12]. Using conventional time-stepping simulations and waiting time for the possible steady state is often not practical because in most cases the time constants of the modes are much larger than the switching period [13]. In the conventional method of

DC-DC converter analysis, steady state ripple values are negligible, compared to the steady state values themselves. Switching power converters are inherently nonlinear, and consequently, it is challenging to calculate the root-mean-square (RMS) values of the state variable ripple. These RMS values are essential in order to calculate the current stresses of the different power converter devices as well as to filter design in order to meet the given specifications [14]. Though power electronic handbook [1] shows the RMS calculation using approximation linear ripple, the result is not entirely correct due to a linear approximation. In order to achieve high performance, proper design, and control, it is necessary to have an exact model of converter [15, 16]. High accuracy is one of the significant features of good modeling [16].

The DC-DC converter analysis can be classified into two categories, numeric and symbolic analysis. The references [12, 13, 15, 17–20] shows the numeric analysis. The analysis observes the system response by entering the parameter values into the model. The numeric analysis needs some computation-time to show the output response. The equation does not describe the relationship between each parameter. The numeric analysis observes the relation between parameter by comparing the parameter change to output change.

The [12] construct impedance or admittance matrix of DC-DC converter. Newton-Raphson calculates the output response of the converter. The technique solves the steady-state output per fixed time-step (fixed sampling interval). The accuracy of analysis is dependent on time-step. Few sampling points cause inaccuracy. On the other side, more sampling points need more calculation time. The [18] substitutes original circuit with periodically switched linear (PSL) circuit. Fourier series can observe the PSL. The paper uses 110 as sequence numbers in Fourier series summation. The [19] also uses Fourier series to simulate steady-state response. Comparing with [18], the [19] only uses 21 sequences. The [18] applies Fourier series of current switching part. The Fourier series of switching part substitutes the original part to be analyzed by Kirchhoff Voltage and Current Law. The paper uses 180 sequence numbers to draw a steady state response of the system [17]. The [17] analyzes the buck converter in the frequency domain due to high accuracy compared with conventional time-domain. The paper simulates three different sequences number that 0, 10 and 100. The paper shows that 10th sequences order is enough to describe steady-state response. In Fourier series based method, great number send the accurate steady-state model, but it needs some calculations. High order sequence number does not bring significant accuracy. Determination of the proper sequence number is another problem besides the main steady-state analysis problem.

Contrary with numerical analysis, symbolic analysis describes the relation be-

tween parameter and output in the equation. The relation between parameter and output can be observed roughly by the equation. The references [14] and [16] discuss the symbolic analysis. Symbolic analysis is complicated although it shows the relation between parameter and output in the equation. The [14] performs steady state symbolic analysis to calculate the RMS value. The paper shows the solution in a matrix form that is more complicated than an ordinary equation. The average and RMS calculation include a term which assumes zero derivation of the state. Since the ripple exists, this assumption contrast with the early definition. The [16] solves the steady-state equation by Laplace transform and reverts into time-domain by the inverse of the Laplace transform. The solution needs the initial value. The paper uses Z-transform due to the similarity between the initial value and last value in one period. Though the paper shows symbolic analysis, the process is long enough due to the calculation of three transformations (Laplace transform, Z-transform and the inverse of the Laplace transform).

This chapter proposes an alternative method that accurately predicts and analyzes the steady state of the switching power converter. The proposed method based on Fourier series since many references show the accuracy [17–19]. The recovery function is also proposed to generate analysis without dependent in some sequences orders. The chapter is subdivided into several sections to present a clear explanation. Section 2.2 shows that the buck converter is like an LTI system. Section 2.3 shows the basic idea of the proposed method. Section 2.4 and 2.5 explain the necessary equation to realize the idea of the steady-state model. Section 2.6 presents the complete steady-state model. Section 2.7 shows the proposed steady-state function by circuit simulation. Finally, Section 2.8 declares the summary of this chapter.

2.2 Linear Time-invariant of Buck Converter

This section shows how a buck converter can be analyzed just like a linear time-invariant (LTI) system. An LTI system has general representation as follows.

$$\dot{x}(t) = Ax(t) + Bu(t) \tag{2.1}$$

Where x is state variable and u is an input. The LTI system has a general solution shown as follows.

$$x(t) = e^{At}x(0) + \int_0^t e^{A(t-\tau)}Bu(\tau)d\tau \tag{2.2}$$

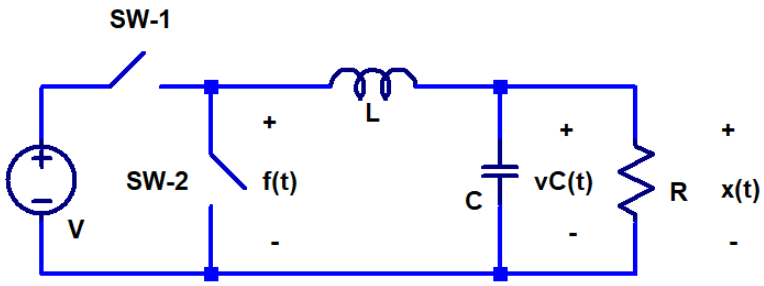

Figure 2.1: Buck converter circuit

Where $x(0)$ is an initial state of the LTI system. The subsection 1.3.5 describes the detail explanation about the solution of the LTI system.

Figure 2.1 shows a buck converter circuit. The converter consists of a pair of switches and an RLC circuit as shown in Figure 1.12. If there is a voltage source can represent the pair of switches, a buck converter is like a linear time-invariant (LTI) system. One possible technique is averaging the voltage between two switches $f(t)$. The following equation expresses the voltage between two switches.

$$f(t) = \begin{cases} V & (0 \leq t < TD) \\ 0 & (TD \leq t < T) \end{cases}, \quad f(t) = f(t+T) \tag{2.3}$$

Then, the average of $f(t)$ is calculated as follows.

$$\bar{f(t)} = \frac{1}{T}\int_0^T g(t)dt = \frac{1}{T}\int_0^{TD} Vdt = VD \tag{2.4}$$

The definition of $\bar{f(t)}$ can simplify the buck converter into Figure 2.2.

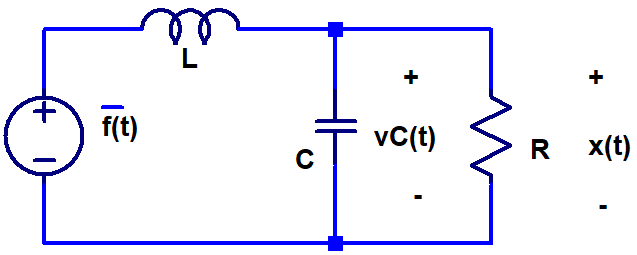

Figure 2.2: Simplified circuit of the buck converter

The state space equation of the simplified buck converter is as follows.

$$\begin{bmatrix} \dot{i_L} \\ \dot{v_C} \end{bmatrix} = \begin{bmatrix} 0 & \frac{-1}{L} \\ \frac{1}{C} & \frac{-1}{RC} \end{bmatrix} \begin{bmatrix} i_L \\ v_C \end{bmatrix} + \begin{bmatrix} \frac{V}{L} \\ 0 \end{bmatrix} D \tag{2.5}$$

In the buck converter, the input only comes from a duty ratio D. The equation (2.5) shows that the simplified buck converter model is similar with an LTI system in the equation (2.1). It means that the buck converter control problem can be solved using a common control technique of the LTI system.

2.3 Steady State Model

This section discusses how to generate a steady state model of an LTI system. An exponential input is given in $u(t) = e^{jn\omega t}$. The LTI system in equation (2.1) uses the exponential input. The general solution of the system (2.2) becomes the following equation.

$$\begin{aligned} x(t) &= e^{At}x(0) + \int_0^t e^{A(t-\tau)}Be^{jn\omega\tau}d\tau \\ &= e^{At}x(0) + \int_0^t e^{At+A(jn\omega I-A)\tau}Bd\tau \\ &= e^{At}x(0) + (jn\omega I - A)^{-1}\left[e^{At+(jn\omega I-A)\tau}\right]_{\tau=0}^{\tau=t}B \\ x(t) &= e^{At}x(0) + (jn\omega I - A)^{-1}\left[e^{jn\omega tI} - e^{At}\right]B \end{aligned} \tag{2.6}$$

If the system is A-stable, then $e^{A\infty} = 0$. The steady state response happens when the system is at $t = \infty$. Then, the steady state model $x_{ss}(t)$ becomes the following equation.

$$x_{ss}(t) = (jn\omega I - A)^{-1}Be^{jn\omega t} \tag{2.7}$$

2.4 Transfer Function of Buck Converter

In the linear time-invariant (LTI) system, the transfer function is usually used to analyze the response of the system in the frequency domain. The transfer function is a ratio of output to the input in the frequency domain. A time domain equation on an LTI system (2.1) can be represented in the frequency domain using a Laplace transform as follows.

$$sX(s) = AX(s) + BU(s) \tag{2.8}$$

If we determine the output is the state variable, the transfer function is calculated as follows.

$$\frac{X(s)}{U(s)} = G(s) = (sI - A)^{-1}B \tag{2.9}$$

New equality is given in $s = jn\omega$. Using a transfer function and input function $u(t) = e^{jn\omega t}$, the steady state model in equation (2.7) can be rewritten as follows.

$$x_{ss}(t) = G(jn\omega t)u(t) \tag{2.10}$$

Based on equation (2.10), the steady-state model requires the transfer function of the buck converter and the exponential input. The input is $f(t)$, and the output is capacitor voltage $v_C(t)$ as shown in the simplified buck converter (Figure 2.2). Then, the transfer function of the buck converter is derived as follows.

$$\begin{aligned} G(s) = \frac{V_C(s)}{F(s)} &= \frac{\frac{1}{sC}||R}{sL + (\frac{1}{sC}||R)} \\ &= \frac{\frac{1}{LC}}{s^2 + \frac{1}{RC}s + \frac{1}{LC}} \end{aligned} \tag{2.11}$$

The transfer function (2.11) has two poles. Here, the dissertation assumes that the poles are complex conjugate pairs ($s = \xi\omega \pm j\eta\omega$), that is,

$$\left(\frac{1}{R^2C^2} - \frac{4}{LC}\right) < 0. \tag{2.12}$$

The transfer function becomes as follows.

$$\begin{aligned} G(s) &= \frac{\frac{1}{LC}}{(s - \xi\omega - j\eta\omega)(s - \xi\omega + j\eta\omega)} \\ &= \frac{\frac{1}{LC}}{s^2 - 2\xi\omega s + (\xi\omega)^2 + (\eta\omega)^2} \end{aligned} \tag{2.13}$$

The next step applies ($s = jn\omega$) to the transfer function as shown in the following equation.

$$\begin{aligned} G(jn\omega) &= \frac{\frac{1}{LC}}{-(n\omega)^2 - 2jn\xi\omega^2 + (\xi\omega)^2 + (\eta\omega)^2} \\ &= \frac{\frac{1}{LC}}{(jn\omega - \xi\omega)^2 + (\eta\omega)^2} \end{aligned} \tag{2.14}$$

The transfer function at $s = 0$ is a DC-gain. The following equation shows how to

calculate the DC-gain.

$$G(0) = \frac{\frac{1}{LC}}{0^2 + \frac{1}{RC}0 + \frac{1}{LC}} = 1 \tag{2.15}$$

The further analysis can use the transfer function to find the steady state model of buck converter.

2.5 Fourier Series Representation

Many phenomenons studied in electric circuit are periodic in nature when time goes to infinity. These periodic functions in time t are representable in Fourier series as follows [21].

$$f(t) = \gamma_0 + \sum_{n\neq 0} \gamma_n e^{jn\omega t} = ... + \gamma_{-2}e^{-j2\omega t} + \gamma_{-1}e^{-j\omega t} + \gamma_0 + \gamma_1 e^{j\omega t} + \gamma_2 e^{j2\omega t} + ... \tag{2.16}$$

where

$$\gamma_0(f) = \frac{1}{T}\int_0^T f(t)dt,\ \gamma_n(f) = \frac{1}{T}\int_0^T f(t)e^{-jn\omega t}dt \tag{2.17}$$

where T is the period and ω is the angular frequency defined by $\omega = \frac{2\pi}{T}$.

A simplified model of buck converter (Figure 2.2) has a square-wave input $f(t)$ represented in the equation (2.3). The input $f(t)$ is a periodic signal which is representable in a Fourier series. The following equations calculate the Fourier coefficients of the input $f(t)$.

$$\begin{aligned}
\gamma_0(f) &= \frac{1}{T}\left(\int_0^{TD} V dt + \int_{TD}^{T} 0 dt\right) = VD, \\
\gamma_n(f) &= \frac{1}{T}\left(\int_0^{TD} V e^{-jn\omega t} dt + \int_{TD}^{T} 0 e^{-jn\omega t} dt\right) \\
&= \frac{1}{T}\left[\frac{V}{-jn\omega}e^{-jn\omega t}\right]_{t=0}^{t=TD} \\
&= \frac{V}{jn\omega T}\left(1 - e^{-jn2\pi D}\right)
\end{aligned} \tag{2.18}$$

Then, Fourier series of $f(t)$ is as follows.

$$f(t) = VD + \sum_{n\neq 0} \frac{V}{jn2\pi}\left(1 - e^{-jn2\pi D}\right)e^{jn\omega t} \tag{2.19}$$

Fourier series gives us another representation of input signal $f(t)$ in an exponential function. The representation shows that the buck converter can be analyzed using equation (2.7) since the input is a summation of exponential function

2.6 Proposed Steady State Model of Buck Converter

This section combines several equations obtained from previous sections to generate the accurate steady-state model of the buck converter. The previous sections represent the input signal into a summation of several exponential functions. It also needs to multiply each exponential function with the corresponding transfer function, so the equation (2.10) becomes the following equation.

$$x_{ss}(t) = G(0)\gamma_0(u) + \sum_{n\neq 0} G(jn\omega)\gamma_n(u)e^{jn\omega t} \tag{2.20}$$

In the previous section, the equation (2.19) explains Fourier series of the input function. The following equation proposes a steady-state model by assuming that $q = jn$ and substituting (2.19), (2.14), and (2.15) into (2.10).

$$\begin{aligned} x_{ss}(t) &= G(0)\gamma_0(f) + \sum_{n\neq 0} G(jn\omega)\gamma_n(f)e^{jn\omega t} \\ &= VD + \sum_{n\neq 0}\left(\frac{\frac{1}{\omega^2 LC}}{(q-\xi)^2+\eta^2}\right)\left(\frac{g}{2\pi q}(1-e^{-2\pi qD})\right)e^{q\omega t} \\ &= VD + \sum_{n\neq 0}\left(\frac{V}{2\pi\omega^2 LC}\right)\left(\frac{1}{(q-\xi)^2+\eta^2}\right)\left(\frac{1}{q}\right)(1-e^{-2\pi qD})e^{q\omega t} \end{aligned} \tag{2.21}$$

The series in the equation (2.21) is complicated. This model cannot explain the relationship between the constant of the circuit to the steady-state output. Rather than use an infinity summation form, this section proposes expression the steady-state model in summation of a special function called recovery function. The complicated model (2.21) will be decomposed into some summations of Fourier series which refer to the recovery functions. Then, we can replace each summation with the corresponding recovery function.

2.6.1 Recovery Function

The infinite series of equation (2.21) is representable in another periodic function. This subsection introduces several special functions named recovery function. The

recovery function is as follows.

$$\begin{aligned} f_{saw}(t) &= \pi - \omega t, && (0 \le t < T), \\ f_c(t) &= \frac{\xi}{\xi^2+\eta^2} + \pi\frac{e^{\xi(\omega t-2\pi)}\cos(\eta\omega t) - e^{\xi\omega t}\cos(\eta(\omega t-2\pi))}{\cosh(2\pi\xi)-\cos(2\pi\eta)}, && (0 \le t < T), \\ f_s(t) &= \pi\frac{e^{\xi(\omega t-2\pi)}\sin(\eta\omega t) - e^{\xi\omega t}\sin(\eta(\omega t-2\pi))}{\cosh(2\pi\xi)-\cos(2\pi\eta)} - \frac{\xi}{\xi^2+\eta^2}, && (0 \le t < T) \end{aligned} \tag{2.22}$$

The equation (2.17) describes Fourier coefficients of recovery functions. By assuming $q = jn$, Fourier series of proposed recovery function becomes as follows.

$$\begin{aligned} f_{saw}(t) &= \sum_{n\neq 0} \gamma_n(f_{saw}) e^{q\omega t} \\ f_c(t) &= \sum_{n\neq 0} \gamma_n(f_c) e^{q\omega t} \\ f_s(t) &= \sum_{n\neq 0} \gamma_n(f_s) e^{q\omega t} \end{aligned} \tag{2.23}$$

where

$$\begin{aligned} \gamma_n(f_{saw}) &= \frac{1}{q} && , \gamma_0(f_{saw}) = 0 \\ \gamma_n(f_c) &= \frac{q-\xi}{(q-\xi)^2+\eta^2} && , \gamma_0(f_c) = 0 \\ \gamma_n(f_s) &= \frac{\eta}{(q-\xi)^2+\eta^2} && , \gamma_0(f_s) = 0 \end{aligned} \tag{2.24}$$

The recovery functions are special because their γ_0 are always zero. This fact makes the decomposition by recovery function does not affect the DC-gain of the transfer function.

2.6.2 Time-delay Function

The decomposition of function sometimes requires the knowledge of time delay characteristic. The following function describes the time-delay function.

$$\tilde{f}(t) = f(t - Th) \tag{2.25}$$

where T is periodic time and h is time delay constant. The following equation simplify the Fourier coefficients of time delay

$$\gamma_n(\tilde{f}) = e^{-q2\pi h}\gamma_n(f). \tag{2.26}$$

This information is useful for the next analysis.

2.6.3 Complete Steady State Model

Principally, the recovery functions (2.22) and their Fourier representation (2.23) is interchangeable. The recovery functions can solve the complicated steady-state model of the buck converter. The following equation decomposes the summation part of the equation (2.21) partially.

$$\begin{aligned}\left(\frac{1}{(q-\xi)^2+\eta^2}\right)\left(\frac{1}{q}\right) &= \frac{1}{(\eta^2+\xi^2)}\left(\frac{1}{q}+\frac{-q+2\xi}{(q-\xi)^2+\eta^2}\right)\\ &= \frac{1}{\eta^2+\xi^2}\left(\frac{1}{q}-\frac{q-\xi}{(q-\xi)^2+\eta^2}+\left(\frac{\xi}{\eta}\right)\frac{\eta}{(q-\xi)^2+\eta^2}\right)\end{aligned} \tag{2.27}$$

The decomposition can be done using a mathematical software such as Wolfram Mathematica 10. The command to decompose an equation is `Apart[]`. The next step of calculation substitute (2.27) in (2.21)as follows.

$$x_{ss}(t) = VD+m\sum_{n\neq 0}\left[\left(\frac{1}{q}-\frac{q-\xi}{(q-\xi)^2+\eta^2}+\mu\frac{\eta}{(q-\xi)^2+\eta^2}\right)(1-\mathrm{e}^{-2\pi qD})\mathrm{e}^{q\omega t}\right] \tag{2.28}$$

where

$$m = \frac{V}{2\pi\omega^2 LC(\eta^2-\xi^2)},\ \mu = \frac{\xi}{\eta}. \tag{2.29}$$

By assuming $q = jn$, the equation (2.28) may become as in the following.

$$\begin{aligned}x_{ss}(t) = VD &+ m\sum_{n\neq 0}\frac{1}{q}(1-\mathrm{e}^{-2\pi qD})\mathrm{e}^{q\omega t} - m\sum_{n\neq 0}\frac{q-\xi}{(q-\xi)^2+\eta^2}(1-\mathrm{e}^{-2\pi qD})\mathrm{e}^{q\omega t}\\ &+ m\mu\sum_{n\neq 0}\frac{\eta}{(q-\xi)^2+\eta^2}(1-\mathrm{e}^{-2\pi qD})\mathrm{e}^{q\omega t}\end{aligned} \tag{2.30}$$

$$
\begin{aligned}
x_{ss}(t) = VD + m & \left(\underbrace{\sum_{n\neq 0} \gamma_n(f_{saw}) \mathrm{e}^{q\omega t}}_{f_{saw}(t)} - \underbrace{\sum_{n\neq 0} \gamma_n(f_{saw}) \mathrm{e}^{-2\pi qD} \mathrm{e}^{q\omega t}}_{f_{saw}(t-TD)} \right) \\
- m & \left(\underbrace{\sum_{n\neq 0} \gamma_n(f_c) \mathrm{e}^{q\omega t}}_{f_c(t)} - \underbrace{\sum_{n\neq 0} \gamma_n f_c \mathrm{e}^{-2\pi qD} \mathrm{e}^{q\omega t}}_{f_c(t-TD)} \right) \\
+ m\mu & \left(\underbrace{\sum_{n\neq 0} \gamma_n(f_s) \mathrm{e}^{q\omega t}}_{f_s(t)} - \underbrace{\sum_{n\neq 0} \gamma_n(f_s) \mathrm{e}^{-2\pi qD} \mathrm{e}^{q\omega t}}_{f_s(t-TD)} \right)
\end{aligned}
\tag{2.31}
$$

The equation (2.31) is easy to be understood if it uses the recovery functions as (2.22). Finally, the following equation proposes an accurate steady-state model of the buck.

$$
\begin{aligned}
x_{ss}(t) = & VD + m\Big(f_{saw}(t) - f_{saw}(t-TD) \Big) - m\Big(f_c(t) - f_c(t-TD) \Big) \\
& + m\mu \Big(f_s(t) - f_s(t-TD) \Big)
\end{aligned}
\tag{2.32}
$$

The proposed equation (2.32) covers an infinite series with the recovery functions. The relationship between each constant of the buck converter is described explicitly in a mathematical equation.

2.7 Simulation Result

This section shows our proposed function (2.32) result and SPICE (Simulation Program with Integrated Circuit Emphasis) using similar constant. The numerical parameter of the DC-DC converter is determined as shown in Table 2.1.

The numerical parameter of resistance (R), inductance (L) and capacitance (C) give complex conjugate poles. Numerical calculation utilized mathematical software (e.g., Wolfram Mathematica 10) to plot the proposed steady-state response. SPICE simulates the circuit responses. Figure 2.3a shows the complete response of the capacitor voltage by parameter-1. Numerical calculation of the proposed method is plotted in solid-line while SPICE results in dashed-line. Figure 2.3b magnifies the steady-state response of parameter-1. Comparison between numerical calculation of proposed function and steady state of SPICE result has

Table 2.1: Numerical parameter

Variable	Parameter-1	Parameter-2
Resistance (R)	6.35 Ω	1.81 Ω
Inductance(L)	100 μH	285 μH
Capacitance (C)	62.7 μF	21.9 μF
Time-period (T)	50 μs	20 μs
Voltage source (g)	10 V	15 V
Duty-ratio (d)	0.5	0.5
Pole (s)	-0.0101 $\pm$ j0.1	-0.0402 $\pm$ j0.0034

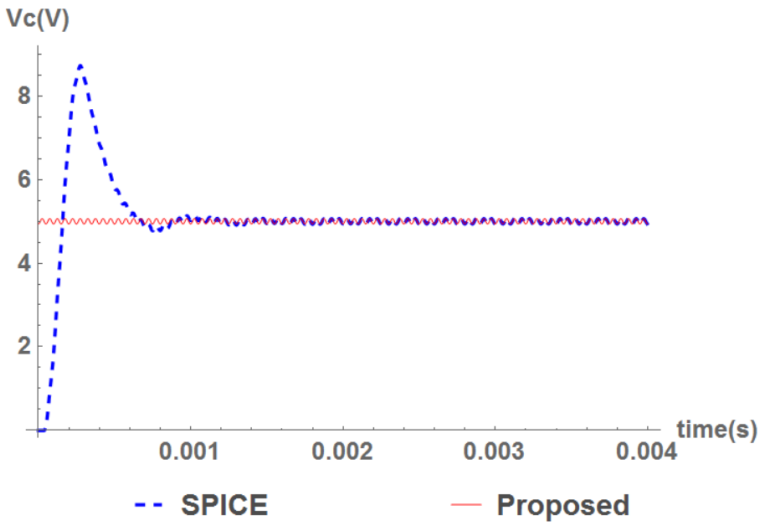

(a) Complete response

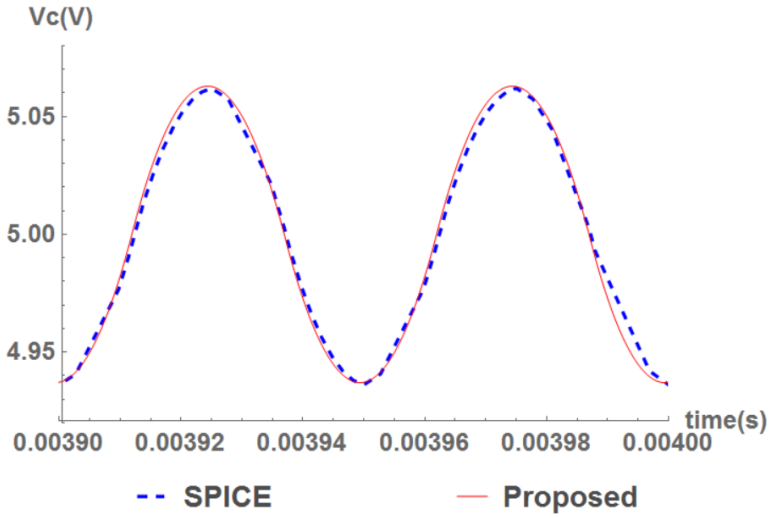

(b) Steady state response

Figure 2.3: Comparison between SPICE and proposed analysis of parameter-1

similarity in shape and value.

Figure 2.4a shows the other complete response of circuit simulation using parameter-2. Figure 2.4b compares the steady state of SPICE and the proposed

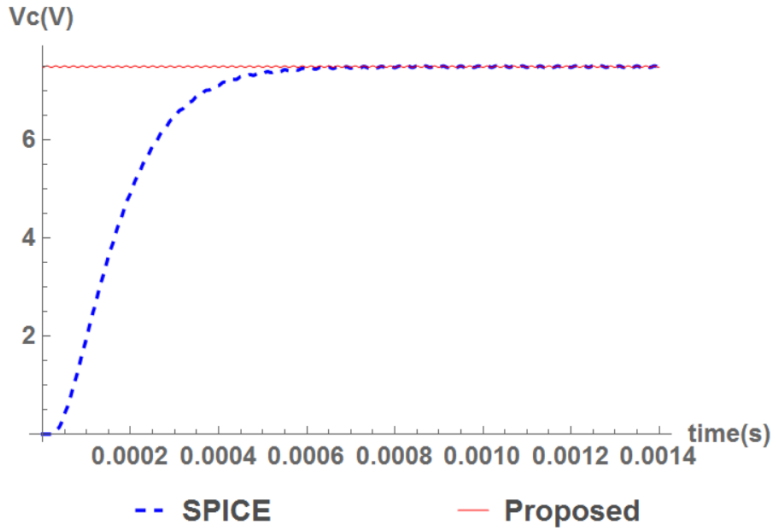

(a) Complete response

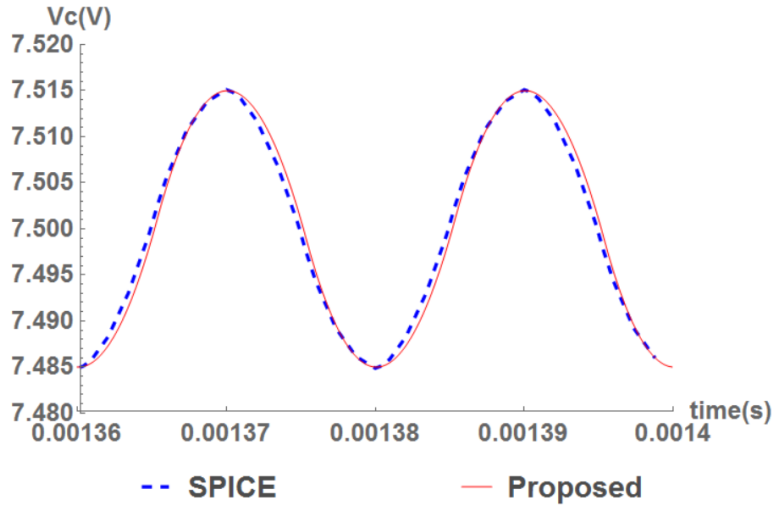

(b) Steady state response

Figure 2.4: Comparison between SPICE and proposed analysis of parameter-2

model in detail. Figure 2.3b and 2.4b describe that numerical calculation of proposed methods gives a consistent result with SPICE result. The proposed method has an advantage in obtaining steady state response without waiting transient time.

2.8 Summary

This chapter has shown that the proposed method describes a steady-state response directly without calculating the transient response. The proposed steady-state model gives an exact symbolical solution of steady-state output. The transition between each mode is described clearly using the proposed method. The recovery function gives an accurate solution of the steady-state model and de-

scribes the relationship of the circuit constant mathematically. The SPICE result approached the proposed model which predicted the steady-state response in advance. Moreover, the proposed method makes the calculation of average and root-mean-square (RMS) traceable

Chapter 3

A Novel Nonlinear Control of Boost Converter using CCM Phase Plane

3.1 Background

Over the last few decades, DC-DC converters have been the subject of great interest due to its large increment of utilization in different applications. Right now, they are popularized in standard and redone items that power an extensive variety of applications, for example, photovoltaic (PV) power systems [22, 23], wind turbines (WT) [24, 25], brushless DC (BLDC) motor [26, 27], and the others. Among these converters, the boost converter is a fundamental controller which many systems use it due to its simplicity.

In order to achieve the operating point, boost converter usually works with the controller techniques. There are two types of controllers for the DC-DC converter as pulse-width modulation (PWM) and phase-shift modulation (PSM). The PWM has been widely utilized to control DC-DC converter in several applications. In the case of less number of components usage and high-reliability demand, the PWM control shows the better performance than PSM [28]. Proportional-integral-derivative (PID) and sliding-mode control (SMC) are used widely in a DC-DC converter. The PID control offers the excellent stability system, but it only operates on the limited operating point. The SMC provides larger operating point than PID. The SMC works well at the most operating point. However, the fundamental barrier for SMC execution is a marvel called 'chattering.'

Based on conduction mode, there is two analysis of the DC-DC converters which are continuous conduction mode (CCM) and discontinuous conduction mode (DCM). The CCM is the most often used in DC-DC converter analysis to design a controller. Although the analysis often chooses the CCM, none of the previous literature examines that their proposed controller works only on CCM region. Since

the design is in the CCM, the controller and the system should work only in that region, or the analysis and design may mislead the controller. Moreover, the controller of the boost converter should be able to handle any operating points with the correct design.

The rapid development of the enormous scale integrated circuit technology brings a digitally controlled DC-DC converter as a hot topic [29]. Digital processors also have the advantage of being less susceptible to aging and environmental or parameter variations. Also, the processor can monitor the system, perform self-diagnostics and tests, and communicate status to a display or a host computer [30]. Implementation of digital controller requires system analysis in the discrete time domain.

This chapter proposes a nonlinear controller of boost converter which can handle any initial points and keep the system always works in CCM. This chapter manipulates the phase portrait of the system to design the proposed controller. The phase portrait has an advantage that it can observe the system response in any initial conditions. This chapter focuses on the boost converter but the other converter can apply the idea. This chapter consists of several sections. Section 3.2 explains the analysis of the boost converter in discrete time-domain which is useful in the implementation of the digital controller. Section 3.3 declares the control system specification in CCM of Boost converter. Section 3.5 proposes the nonlinear control which its design based on the phase portrait examination of any initial condition. Section 3.6 simulates the system on some initial points. The experimental verifies the proposed controller in Section 3.7. Finally, Section 3.8 summarizes the critical point of this chapter.

3.2 Dynamic Model of Boost Converter

This section analyses the dynamic behavior of boost converter. The model of boost converter in discrete time domain will be the aim of this section. In order to derive the discrete model, the analysis starts from a continuous time domain analysis.

3.2.1 Continuous Time Domain Analysis

The boost converter is consisted of an inductor L, a capacitor C, a MOSFET M and a diode D as shown in Figure 3.1. The circuit equation can be derived as follows.

$$\begin{cases} V &= L\dot{i}(t) + v_M(t), \quad v_M(t) &= v_D(t) + v(t) \\ i(t) &= i_M(t) + i_D(t), \quad i_D(t) &= C\dot{v}(t) + \frac{v(t)}{R} \end{cases} \tag{3.1}$$

The capacitor voltage, inductor current, diode voltage and MOSFET voltage are

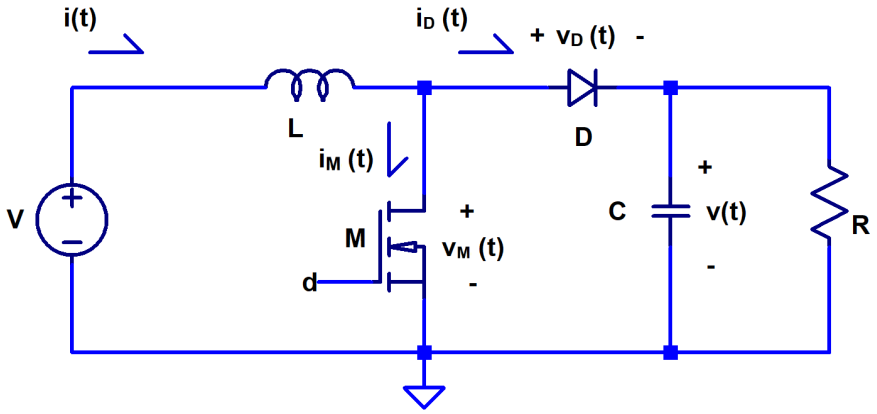

Figure 3.1: Boost converter

denoted as $v(t)$, $i(t)$, v_D and v_M respectively. The boost converter connects with a resistive load R. A source V supplies a constant voltage for boost converter. The switching mode is controlled by duty-ratio d of PWM.

In CCM, there are two modes which work alternately. In the first mode called as *mode-1*, the MOSFET M is active, and the diode D is disconnected. We assume that the MOSFET voltage is constant V_M during mode-1 and there is no current on the diode ($i_D(t) = 0$). The second mode named as *mode-2* occurs while the MOSFET is off and the diode is on. We assume that the diode voltage is constant V_D and there is no current on MOSFET ($i_M(t) = 0$) during mode-2. The equation of the boost converter becomes as follows

$$\text{Mode-1} \begin{cases} L\dot{i}(t) &= V - V_M \\ C\dot{v}(t) &= -\frac{v(t)}{R} \end{cases} \tag{3.2}$$

$$\text{Mode-2} \begin{cases} L\dot{i}(t) &= V - V_D - v(t) \\ C\dot{v}(t) &= i(t) - \frac{v(t)}{R}. \end{cases} \tag{3.3}$$

In this subsection, we introduce a non-dimensional variable x_1 and x_2 which is described as follows.

$$\begin{cases} x_1 &= \frac{v(t)-V+V_D}{V} \\ x_2 &= \frac{i(t)}{V}\sqrt{\frac{L}{C}} \end{cases}, \quad \begin{cases} v(t) &= Vx_1 + V - V_D \\ i(t) &= V\sqrt{\frac{C}{L}}x_2 \end{cases} \tag{3.4}$$

By substituting $\dot{i}(t)$ and $\dot{v}(t)$ of (3.2) and (3.3), the derivative of non-dimensional

state is written in the following equations.

$$\text{mode-1}\begin{cases} \dot{x_1} & = \frac{\dot{v(t)}}{V} = \frac{1}{V} \times \frac{-(Vx_1+V-V_D)}{RC} & = -\frac{1}{RC}x_1 - \frac{1}{RC}\left(1-\frac{V_D}{V}\right) \\ \dot{x_2} & = \frac{\dot{i(t)}}{V}\sqrt{\frac{L}{C}} = \frac{1}{V}\sqrt{\frac{L}{C}} \times \left(\frac{V-V_M}{L}\right) & = \frac{1}{\sqrt{LC}}\left(1-\frac{V_M}{V}\right) \end{cases} \tag{3.5}$$

$$\text{mode-2}\begin{cases} \dot{x_1} & = \frac{\dot{v(t)}}{V} = \frac{1}{V} \times \left(\frac{i(t)}{C} - \frac{v(t)}{RC}\right) = \frac{1}{\sqrt{LC}}x_2 - \frac{1}{RC}x_1 - \frac{1}{RC}\left(1-\frac{V_D}{V}\right) \\ \dot{x_2} & = \frac{\dot{i(t)}}{V}\sqrt{\frac{L}{C}} = \frac{1}{V}\sqrt{\frac{L}{C}} \times \frac{V-V_D-v(t)}{L} = \frac{-1}{\sqrt{LC}}x_1 \end{cases} \tag{3.6}$$

The state space equation of non-dimensional variable can be written as follows.

$$\dot{x} = \underbrace{\begin{bmatrix} \frac{-1}{RC} & 0 \\ 0 & 0 \end{bmatrix}}_{A_1} x + \underbrace{\begin{bmatrix} \frac{-1}{RC}(1-\frac{V_D}{V}) \\ \frac{1}{\sqrt{LC}}\left(1-\frac{V_M}{V}\right) \end{bmatrix}}_{b_1} \tag{3.7}$$

$$\dot{x} = \underbrace{\begin{bmatrix} \frac{-1}{RC} & \frac{1}{\sqrt{LC}} \\ \frac{-1}{\sqrt{LC}} & 0 \end{bmatrix}}_{A_2} x + \underbrace{\begin{bmatrix} \frac{-1}{RC}(1-\frac{V_D}{V}) \\ 0 \end{bmatrix}}_{b_2} \tag{3.8}$$

Where $x^T = [x_1 \;\; x_2]$. The general solution of state space equation is defined in following equation.

$$\dot{x}(t) = Ax(t) + b, \qquad x(t) = e^{A(t-t_0)}x(t_0) + \int_{t_0}^{t} e^{A(t-p)}bdp \tag{3.9}$$

Where t_0 is a beginning time of the system.

The mode-1 works from the beginning of a period (T) until $t = t_0 + Td$. Based on general solution of state space equation, the last state of mode-1 can be written as follows.

$$x(t_0+Td) = e^{A_1(t_0+Td-t_0)}x(t_0) + \int_{t_0}^{t_0+Td} e^{A_1(t_0+Td-p)}b_1dp$$

$$\text{where}\begin{cases} q = \frac{p-t_0}{T} \\ p = qT + t_0 \\ \frac{dp}{dq} = T \end{cases}$$

$$x(t_0+Td) = e^{A_1Td}x(t_0) + \int_0^d e^{A_1T(d-q)}b_1Tdq \tag{3.10}$$

In CCM, the boost converter has two state-space equations which are (3.7) and (3.8). The last state of mode-1 will become the initial state of mode-2. On the next step, the last state of mode-2 will be equal to the initial state of the next

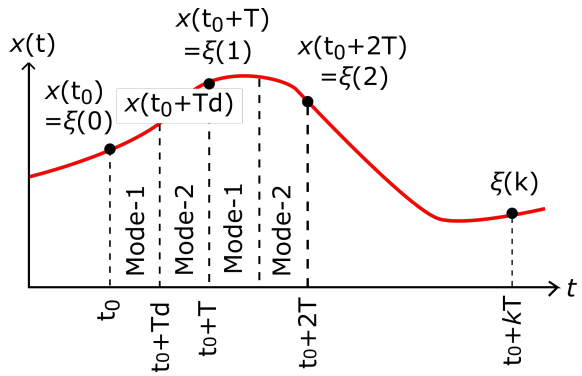

Figure 3.2: Discrete-time of state

period mode-1. These phenomena occur repeatedly. Based on these facts, the solution of the boost converter in one period (T) can be obtained by substituting the last state of mode-1 into the initial state of the mode-2 solution as follows.

$$\begin{aligned} x(t_0+T) &= e^{A_2T(1-d)}x(t_0+Td) + \int_d^1 e^{A_2(t_0+T-(qT+t_0))}b_2Tdq \\ &= e^{A_2T(1-d)}e^{A_1Td}x(t_0) + e^{A_2T(1-d)}\int_0^d e^{A_1T(d-q)}b_1Tdq + \int_d^1 e^{A_2T(1-q)}b_2Tdq \end{aligned} \tag{3.11}$$

3.2.2 Discrete Time Domain Analysis

There is a time-delay between one measurement to another measurement. By considering this situation, the sensor measures is assumed has same sampling-time with switching period T as shown in dot point of Figure 3.2. In this subsection, we will introduce a new variable ξ to distinguish with non-dimensional variable x in continuous-time domain. Then, the discrete representation of solution (3.11) is defined as follows.

$$\begin{aligned} \xi(k+1) &= x\left(t_0+(k+1)T\right) \\ &= e^{\tilde{A}_2(1-d)}e^{\tilde{A}_1d}\underbrace{x(t_0+kT)}_{\xi(k)} + e^{\tilde{A}_2(1-d)}\int_0^d e^{\tilde{A}_1(d-q)}\tilde{b_1}dq + \int_d^1 e^{\tilde{A}_2(1-q)}\tilde{b_2}dq \end{aligned} \tag{3.12}$$

where $\tilde{A_1} = A_1T$, $\tilde{A_2} = A_2T$, $\tilde{b_1} = b_1T$, $\tilde{b_2} = b_2T$ and $\xi^T = [\xi_1 \;\; \xi_2]$.

The new variable is defined to simplify the solution as follows.

$$\varepsilon_1 = \frac{T}{RC},\ \varepsilon_2 = \frac{T}{\sqrt{LC}},\ \alpha = (1-\frac{V_M}{V}),\ \text{and}\ \beta = (1-\frac{V_D}{V}) \tag{3.13}$$

Then, the matrix $\tilde{A_1}$, $\tilde{A_2}$, $\tilde{b_1}$ and $\tilde{b_2}$ can be simplified as follows.

$$\tilde{A_1} = \begin{bmatrix} -\varepsilon_1 & 0 \\ 0 & 0 \end{bmatrix}, \tilde{A_2} = \begin{bmatrix} -\varepsilon_1 & \varepsilon_2 \\ -\varepsilon_2 & 0 \end{bmatrix}, \tilde{b_1} = \begin{bmatrix} -\varepsilon_1\beta \\ \varepsilon_2\alpha \end{bmatrix}, \text{and } \tilde{b_2} = \begin{bmatrix} -\varepsilon_1\alpha \\ 0 \end{bmatrix} \tag{3.14}$$

Assuming the period T is small then the element of $\tilde{A_1}$, $\tilde{A_2}$, $\tilde{b_1}$, and $\tilde{b_2}$ become small too. The exponential part in (3.12) can be calculated using the definition of exponential as follows.

$$e^M \simeq \mathrm{I} + M + \frac{1}{2!}M^2 + ... \tag{3.15}$$

$$e^{\tilde{A_1}d} \simeq \mathrm{I} + \tilde{A_1}d + \underbrace{\frac{\tilde{A_1}^2 d^2}{2} + ...}_{\text{neglected}} = \mathrm{I} + \tilde{A_1}d \tag{3.16}$$

$$e^{\tilde{A_2}(1-d)}e^{\tilde{A_1}d} \simeq \mathrm{I} + \tilde{A_1}d + \tilde{A_2}(1-d) \tag{3.17}$$

$$e^{\tilde{A_2}(1-d)}\int_0^d e^{\tilde{A_1}(d-q)}\tilde{b_1}dq \simeq (\mathrm{I} + \tilde{A_2}(1-d))\int_0^d (\mathrm{I} + \tilde{A_1}(d-q))\tilde{b_1}dq = \tilde{b_1}d \tag{3.18}$$

$$\int_d^1 e^{\tilde{A_2}(1-q)}\tilde{b_2}dq \simeq \int_d^1 (\mathrm{I} + \tilde{A_2}(1-q))\tilde{b_2}dq = \tilde{b_2}(1-d) \tag{3.19}$$

Thus, the discrete-time solution of state (3.12) is simplified as follows

$$\xi(k+1) = \underbrace{(\mathrm{I} + \tilde{A_1}d + \tilde{A_2}(1-d))}_{\hat{A}}\xi(k) + \underbrace{\tilde{b_1}d + \tilde{b_2}(1-d)}_{\hat{b}} \tag{3.20}$$

The equation (3.20) is used to simulate the boost converter and design the controller on the next sections.

3.3 Problem in Boost Converter

After understand how the model of boost converter in discrete time domain, we can simulate the behavior of boost converter using the model. First, this section mentions the specification of controller.

3.3.1 Control Specification

This chapter analyses a boost converter in continuous conduction mode (CCM) only so the controller should have some specification as mention below.

1. The output voltage must be greater than the input voltage. If the output voltage is less than the input voltage, the diode is always on even the MOSFET

is on. On the CCM, the diode should be off when the MOSFET is on and vise verse. The diode becomes uncontrollable. The output voltage $v(t)$ must be higher than the input voltage V subtracted by the diode voltage V_D. In the non-dimensional state, the ξ_1 must never become negative.

2. The inductor current must be positive which means the current flows from input source to the output direction. If the inductor current is negative, both MOSFET and diode may be off and the system becomes DCM. The inductor current $i(t)$ must be greater than zero. In other words, the state ξ_2 must not be a negative value.

Breaking the specification means the model does not proper anymore with the designated controller. Keeping the wrong model may mislead the analysis or controller design.

3.3.2 Boost Converter Behavior

In this subsection, the preliminary simulation is conducted to give a clear illustration about the behavior of boost converter without a controller, called as an open-loop response. Moreover, this subsection shows how the system may break the limitations and why it needs a proper controller. The parameters of boost converter are taken from [31] as shown in Table 3.1. The parameters will be used to compare the PID control technique in [31] with the proposed controller in Section 3.4 and 3.5.

Table 3.1: The parameter of boost converter

Parameter	Symbol	Value
Input voltage	V	10 V
Inductor	L	300 μH
Capacitor	C	100 μF
MOSFET voltage	V_M	162 mV
Diode voltage	V_D	0.5 V
Load	R	10 Ω
Switching period	T	20 μs
Reference voltage	V_{ref}	16 V

Based on Table 3.1, we want to achieve the reference voltage as the output of the boost converter in steady state or equilibrium. The duty ratio, named D_{eq}, need to be known. The steady state occurs when there is no change in the state which are inductor current and output voltage. The model of the boost converter explained in equation (3.20), uses the non-dimensional variable instead of inductor current or output voltage. Thus, we need to represent the reference voltage

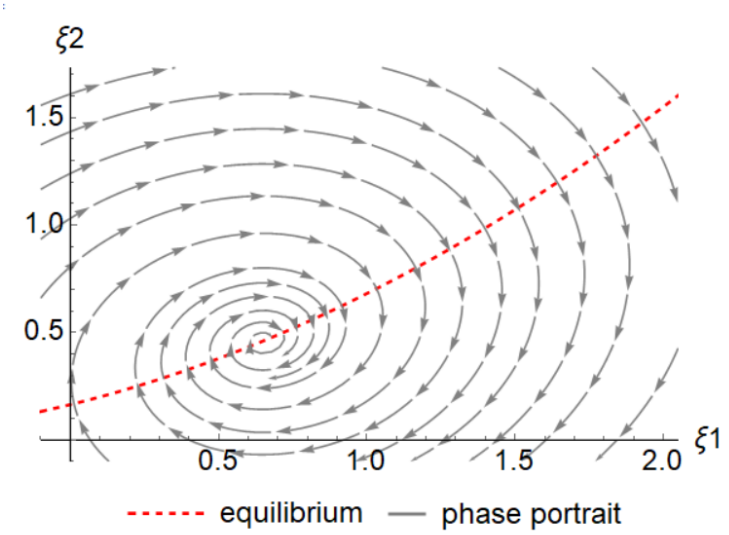

Figure 3.3: Phase portrait of the open-loop response

in a non-dimensional variable also. The reference can be expressed by equation (3.4) in the following equation.

$$\xi_{ref} = \frac{V_{ref} - V + V_D}{V} \tag{3.21}$$

By using ξ_{ref} as ξ_1 in the equation (3.20), the duty ratio can be obtained when the $\xi(k+1)$ is equal to the $\xi(k)$. Using mathematical software, the solution of duty ratio can be obtained as follows.

$$D_{eq} = \frac{\xi_{ref}}{\alpha + \xi_{ref}} \tag{3.22}$$

In order to examine the behavior of boost for any initial condition, the phase portrait is utilized in phase plane. The phase portrait of open-loop response that occurs when the duty ratio d is equal to D_{eq} is shown in Figure 3.3. The arrow shows the direction of non-dimensional variable changing. The figure shows that the system can achieve equilibrium point well for any initial points.

This description focuses on the phase trajectory of two initial points which are A and B in Figure 3.4. The initial point A can achieve the equilibrium point without entering the negative area of the phase plane. The behavior of initial point A means that the system does not break the limitation as described in Sub-section 3.3.1. For the initial condition B, the system enters the negative region of ξ_1 and ξ_2 which breaks the limits of CCM boost converter. In order to avoid this situation, the system requires a proper controller.

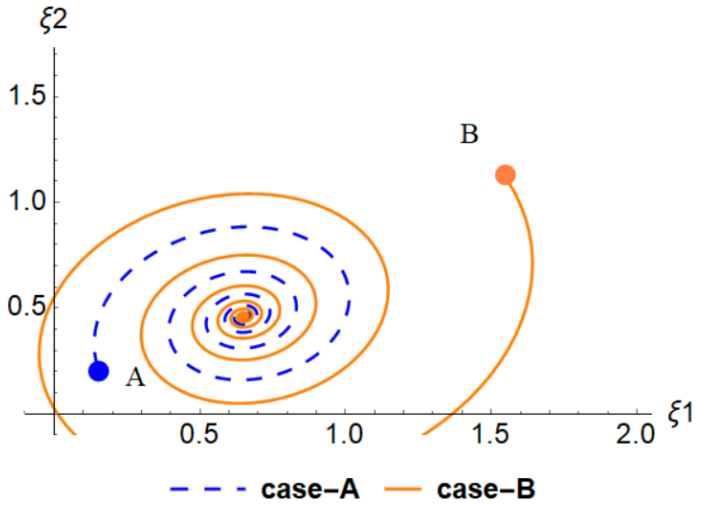

Figure 3.4: Phase portrait of Case-A and Case-B

3.4 Proportional Integral Differential Control

Among the several controllers of the boost converter, proportional integral differential (PID) controller is the mature controller which is well-explained in several papers such as [28, 29, 32–34]. This section discusses the implementation of the PID controller and its characteristic on a boost converter. The design of PID controller usually uses the small-signal model of the DC-DC converter [1]. The small-signal model is derived by adding small perturbation on the inductor current $i(t)$, the capacitor voltage $v(t)$ and the duty-ratio d.

The PID controller in discrete-time domain is expressed as follows [32].

$$u(k) = K_P \left[e(k) + \frac{T}{T_I} \sum_{j=0}^{k} e(j) + \frac{T_D}{T} \{e(k) - e(k-1)\} \right] \tag{3.23}$$

The recursive expression of PID control in discrete-time is formed by difference between simultaneous input ($\Delta u(k) = u(k) - u(k-1)$). The recursive PID control can be expressed as follows [31, 32]:

$$\begin{aligned} u(k) &= u(k-1) + \Delta u(k) \\ &= d(k-1) + (K_P + K_I + K_D)\, e(k) - (K_P + 2K_D)\, e(k-1) + K_D e(k-2) \end{aligned} \tag{3.24}$$

where

$$K_I = \frac{K_P T}{T_I}, \qquad K_D = \frac{K_P T_D}{T}, \qquad e(k) = V_{ref} - v(kT),$$
$$e(k-1) = V_{ref} - v(kT-T), \text{ and} \qquad e(k-2) = V_{ref} - v(kT-2T). \tag{3.25}$$

Since the PID controller is designed by linearization around the equilibrium point, implementation of PID controller needs equilibrium duty-ratio D_{eq} as described in the following equation [33].

$$\begin{aligned} d(k) =& D_{eq} + u(k) = D_{eq} + d(k-1) + (K_P + K_I + K_D)\, e(k) \\ & - (K_P + 2K_D)\, e(k-1) + K_D e(k-2) \end{aligned} \tag{3.26}$$

The behavior of PID controller is examined in the phase plane. The parameter of PID needs to be tuned before used. Based on [34], the Ziegler-Nichols (ZN) has the best performance comparing with the others. The simulation shows that the boost converter achieves ultimate gain (K_U) and ultimate period (T_U) on 0.06 and 1,8 ms respectively. By ZN table on [34], the P-gain (K_P), D-gain (K_D), and I-gain (K_I) are 0.036, 8×10^{-4} and 0.405 respectively.

The phase trajectory of PID controller on several initial condition $v(0)$s and $i(0)$s is drawn in this section. The phase trajectory of PID controller is observed by applying (3.20), (3.22), (3.24), and (3.26) on the several initial points. Figure 3.5 shows the phase trajectory of PID controller for several initial conditions. Based on Figure 3.5, the flow of state tends to go to negative area of ξ_2 at first. Most of the tested initial state enters the negative area of ξ_1 and ξ_2 which breaks the limitation of boost converter in Section 3.3. This fact shows that the PID does not guarantee the boost converter works always in CCM.

3.5 Proposed Controller

The previous section explains that both of open-loop with constant duty-ratio and PID closed-loop break the limitation of the design. This section proposes the nonlinear feedback control which keeps the system to stay in CCM. The proposed controller is designed based on manipulation of phase portrait of the open-loop system. The flow of phase portrait consists of horizontal vector ($\Delta\xi_1 = \xi_1(k+1) - \xi_1(k)$) and vertical vector ($\Delta\xi_2 = \xi_2(k+1) - \xi_2(k)$) based on (3.20). The idea is to force both of vectors into the desired direction. Figure 3.6 illustrates the geometry of the desired direction. Based on the illustration, there is equality ($\Delta\xi_2 \sin\theta - \Delta\xi_1 \cos\theta = 0$) when the flow direction has an angle θ. By finding the duty ratio which is satisfied the equality, the flow can be steered to a certain

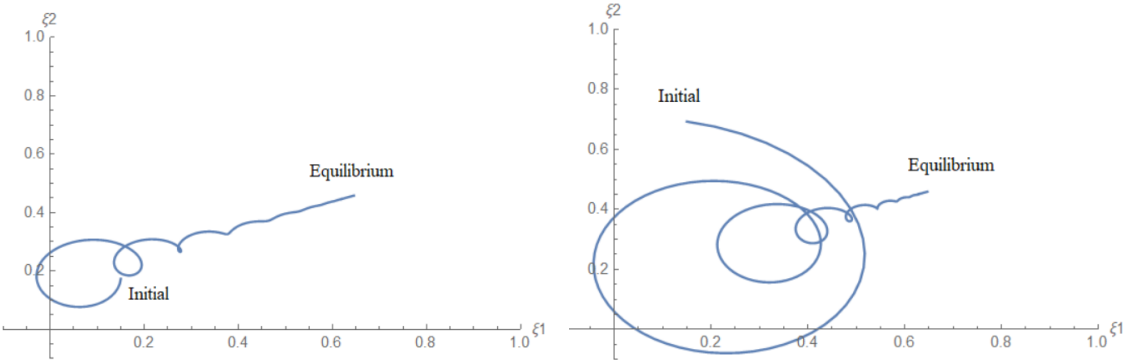

(a) $v(0) = 11\text{V}, i(0) = 1\text{A}$ (b) $v(0) = 11\text{V}, i(0) = 4\text{A}$

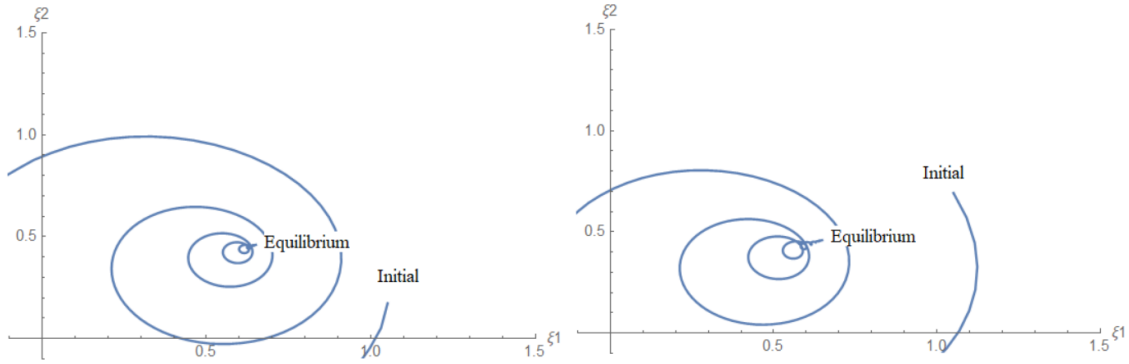

(c) $v(0) = 20\text{V}, i(0) = 1\text{A}$ (d) $v(0) = 20\text{V}, i(0) = 4\text{A}$

Figure 3.5: Phase trajectory of PID controller

direction. Using a mathematical software (e.g., Wolfram Mathematica 10), the solution of duty ratio (d_{mod}) can be solved. The command to solve the equality is `Solve[`$\Delta\xi_2 \sin\theta - \Delta\xi_1 \cos\theta == 0$`,d]`. The solution of equality is as follows.

$$d_{mod}(k) = \frac{\varepsilon_2\xi_1(k)\sin\theta - (\varepsilon_1\beta + \varepsilon_1\xi_1(k) - \varepsilon_2\xi_2(k))\cos\theta}{\varepsilon_2\left[\xi_2(k)\cos\theta + (\alpha + \xi_1(k))\sin\theta\right]} \tag{3.27}$$

The parameter θ in the equation (3.27) needs to be tuned. The desired angle θ is 0.35π. The phase portrait of the system becomes Figure 3.7. The manipulated flows go to the equilibrium curve directly without entering the restricted area or the negative area. However, the flow still does not reach an equilibrium point as occurred in the open-loop system (Figure 3.3). In order to force the flow to go to the equilibrium point, a proportional controller will be added in the control rule. Finally, the proposed nonlinear control is as follows.

$$d_{proposed}(k) = k(\xi_{ref} - \xi_1(k)) + \frac{\varepsilon_2\xi_1(k)\sin\theta - (\varepsilon_1\beta + \varepsilon_1\xi_1(k) - \varepsilon_2\xi_2(k))\cos\theta}{\varepsilon_2\left[\xi_2(k)\cos\theta + (\alpha + \xi_1(k))\sin\theta\right]} \tag{3.28}$$

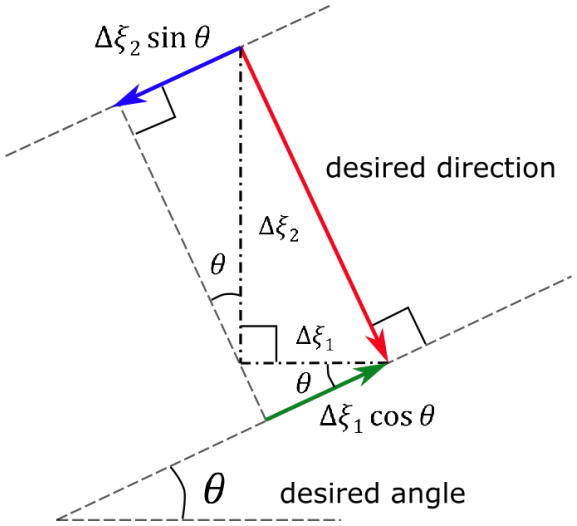

Figure 3.6: The desired direction of the flow

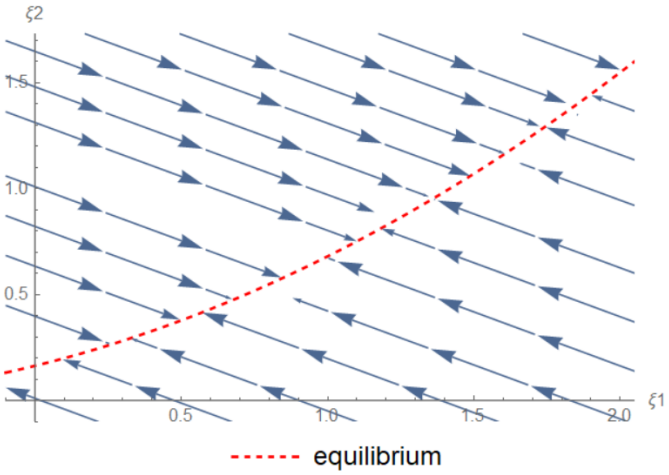

Figure 3.7: Manipulation of the flow

The parameter k also needs to be tuned, which represent speed of achievement reference. The best value of k is 0.06. The phase portrait of proposed controller is shown in Figure 3.8. The phase portrait shows that the controller can handle any initial point to stay in CCM. Any initial point is pushed into equilibrium line without passing the negative area of ξ_1 or the negative area of ξ_2 while achieving the goal.

3.6 Simulation

This section simulates the proposed controller response in the time domain. This section compares the proposed controller in equation (3.28) with the PID controller in equation (3.26). This section simulates several initial points to observe the response of the controller. Figure 3.9 shows the comparison between the pro-

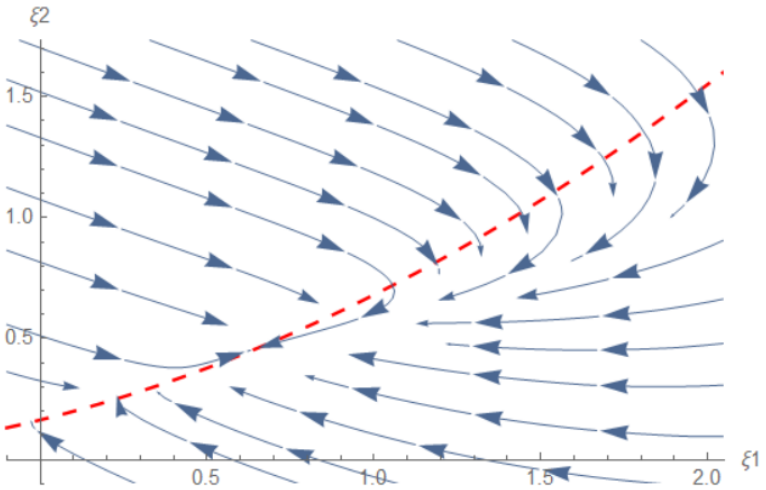

Figure 3.8: Phase plane of proposed controller ($V_{ref} = 16$ V)

posed controller response and the PID controller response. The PID controller response is shown in the dashed red line while the proposed controller is in solid blue line. The proposed controller shows smoother response than the PID controller. In the PID controller, the output voltage goes to under input voltage 10 V. This condition is not proper for boost converter characteristic. The output voltage must be higher than the input voltage. The output voltage must higher than 10 V. Our controller performs a better control which keeps the output always higher than its input voltage.

Moreover, Figure 3.10 shows the phase portrait of the proposed controller on the various reference points. The Figure 3.10 gives clear information that the proposed controller can handle any references point and any initial point without entering the negative area.

3.7 Experiment

The implementation of proposed nonlinear control is discussed in this section to observe whether the idea is implementable or not. The implementation of the controller needs to consider the significant parasitic parameter such as the resistance of the inductor. Therefore, the model of the converter needs to be adjusted, and the controller also needs to be recalculated.

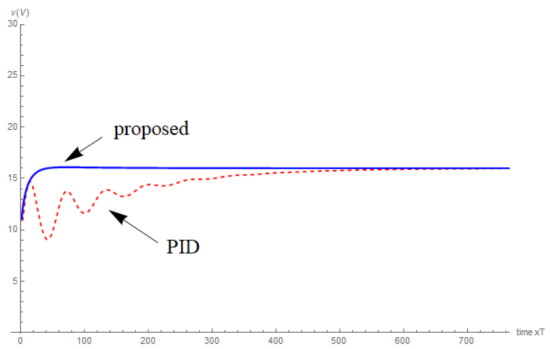

(b) $v(0) = 11\text{V}, i(0) = 1\text{A}$

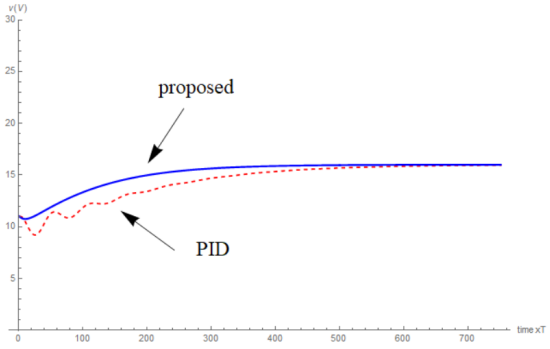

(c) $v(0) = 11\text{V}, i(0) = 4\text{A}$

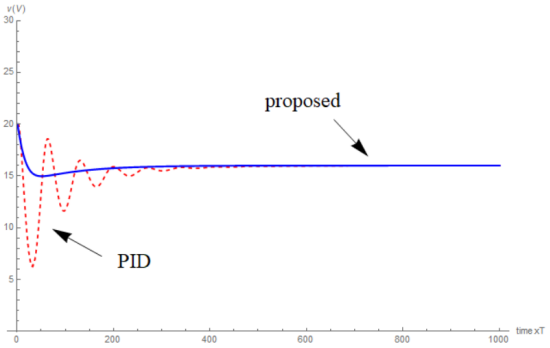

(d) $v(0) = 20\text{V}, i(0) = 1\text{A}$

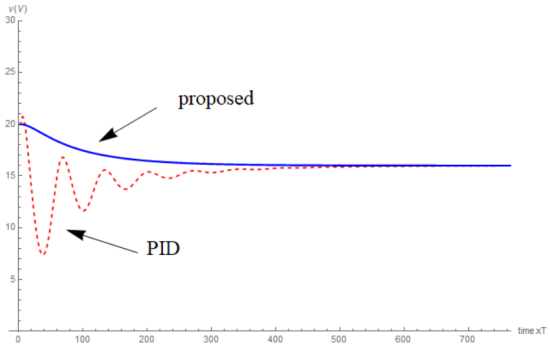

(e) $v(0) = 20\text{V}, i(0) = 4\text{A}$

Figure 3.9: Comparison between proposed and PID on several initial points

3.7.1 Model Adjustment

The existence of significant inductor resistance changes the equation (3.1) to be following equation.

$$\begin{cases} V &= R_L i(t) + L\dot{i}(t) + v_M(t), & v_M(t) &= v_D(t) + v(t) \\ i(t) &= i_M(t) + i_D(t), & i_D(t) &= C\dot{v}(t) + \frac{v(t)}{R} \end{cases} \tag{3.29}$$

Using the similar technique in Section 3.2, the equation (3.29) generates a new definition of A_1, A_2, b_1 and b_2 as follows.

$$\text{mode-1: } \dot{x} = \underbrace{\begin{bmatrix} \frac{-1}{RC} & 0 \\ 0 & \frac{-R_L}{L} \end{bmatrix}}_{A_1} x + \underbrace{\begin{bmatrix} \frac{-1}{RC}(1 - \frac{V_D}{V}) \\ \frac{1}{\sqrt{LC}}\left(1 - \frac{V_M}{V}\right) \end{bmatrix}}_{b_1} \tag{3.30}$$

$$\text{mode-2: } \dot{x} = \underbrace{\begin{bmatrix} \frac{-1}{RC} & \frac{1}{\sqrt{LC}} \\ \frac{-1}{\sqrt{LC}} & \frac{-R_L}{L} \end{bmatrix}}_{A_2} x + \underbrace{\begin{bmatrix} \frac{-1}{RC}(1 - \frac{V_D}{V}) \\ 0 \end{bmatrix}}_{b_2} \tag{3.31}$$

This changes affect the modification of variables $\tilde{A_1}$, $\tilde{A_2}$, $\tilde{b_1}$, and $\tilde{b_2}$ as shown in following equation.

$$\begin{aligned}
\tilde{A_1} &= A_1 T = \begin{bmatrix} -\epsilon_1 & 0 \\ 0 & -\epsilon_3 \end{bmatrix},\ \tilde{b_1} = b_1 T = \begin{bmatrix} -\beta\epsilon_1 \\ \alpha\epsilon_2 \end{bmatrix} \\
\tilde{A_2} &= A_2 T = \begin{bmatrix} -\epsilon_1 & \epsilon_2 \\ -\epsilon_2 & -\epsilon_3 \end{bmatrix},\ \tilde{b_2} = b_2 T = \begin{bmatrix} -\beta\epsilon_1 \\ 0 \end{bmatrix} \\
\epsilon_1 &= \frac{T}{RC},\ \epsilon_2 = \frac{T}{\sqrt{LC}},\ \epsilon_3 = \frac{TR_L}{L} \\
\alpha &= 1 - \frac{V_M}{V},\ \beta = 1 - \frac{V_D}{V}
\end{aligned} \tag{3.32}$$

The flow of phase trajectory consists of horizontal vector ($\xi_1(k+1) - \xi_1(k)$) and vertical vector ($\xi_2(k+1) - \xi_2(k)$) based on equation (3.20). The idea of controller forces the vertical vector to zero and find the solution of duty ratio d in equation (3.20). The solution of the duty-ratio is equal to following equation.

$$d = \frac{\epsilon_2\xi_1 + \epsilon_3\xi_2}{\epsilon_2(\alpha + \xi_1)} \tag{3.33}$$

Adding the proportional part can force the flow to the reference point ξ_{ref}. The proposed control law is modified as follows.

$$d = k(\xi_{ref} - \xi_1) + \frac{\epsilon_2\xi_1 + \epsilon_3\xi_2}{\epsilon_2(\alpha + \xi_1)} \tag{3.34}$$

where

$$\xi_{ref} = \frac{V_{ref} - V - V_D}{V} \tag{3.35}$$

The next subsection uses the controller in equation (3.34) and examines in the experiment. The constant $k = 0.005$ gives the good response for several initial point during the tuning. The next subsection implements the control rule into a micro-controller.

3.7.2 Measurement Result

Table 3.2 shows the detail of the parameter in the experiment. Figure 3.11 shows the experimental setup which consists of the voltage source, a boost converter, sensors, micro-controller, and load. The voltage source utilizes Agilent U8001A Single Output DC Power Supply. This experiment uses Texas Instrument TM4C123GXL which is ARM Cortex-M4 at the 80MHz operating frequency to apply the proposed controller. The controller uses Allegro ACS714 current sensor to get input current

and output current. The boost converter uses K2232 MOSFET and FMX22S diode. The experiment will verify the proposed controller in two initial conditions, called as Case-A and Case-B. This Case-A and Case-B are different from the case in Section 3.6. The output voltage measurement result of Case-A and Case-B are shown in Figure 3.12 and Figure 3.13 respectively. In order to set the system in different initial conditions, the controller generates constant duty-ratio PWM at the beginning until the system is steady before turning on the controller. This experiment puts a constant duty-ratio at the first 20ms. It explains the flat or constant voltage in Figure 3.12 and Figure 3.13 before it goes up or down to reach the reference voltage.

Table 3.2: The experimental parameter of the proposed nonlinear controller

Parameter	Symbol	Value
Input voltage	V	7 V
Inductor resistor	R_L	1.12 Ω
Inductor	L	150 μH
Capacitor	C	220 μF
MOSFET voltage	V_M	400 mV
Diode voltage	V_D	800 mV
Load	R	20 Ω
Switching period	T	100 μs
Reference voltage	V_{ref}	10 V

Figure 3.14-3.17 show the comparisons between simulation and experiment. The simulation results are in a dashed blue line, and the experimental results are in solid orange line. Figure 3.14 and 3.15 shows the output voltage comparison of Case-A and Case-B respectively. Both simulation and experimental result achieve the reference voltage in a steady state. Figure 3.16 and 3.17 show duty-ratio as the output of the controller. Based on Figure 3.16 and 3.17, the proposed controller eliminates the chattering problem which is commonly known in SMC (sliding mode control). In general, the experimental result shows a good agreement with simulation data.

3.8 Summary

This chapter has proposed a model of boost converter based on the general solution of state space equation in each mode. This chapter shows the representation in the discrete-time equation to draw a phase plane and implement the controller in a digital processor. The phase portrait gives a visual trace of system response in any initial conditions and is useful in the controller design. This chapter has pointed out that the PID control does not guarantee that boost converter works

within CCM. This chapter has proposed a novel nonlinear controller, and it guarantees that the boost converter always works in CCM correctly for any initial condition. Moreover, the proposed controller has an advantage more than PID that it can handle any reference point without requiring re-tuning the parameters. The simulation result has shown that the proposed controller works well under different initial conditions. The experiment has verified that the proposed controller is implementable in the hardware. The experiment result showed a good agreement with the simulation result.

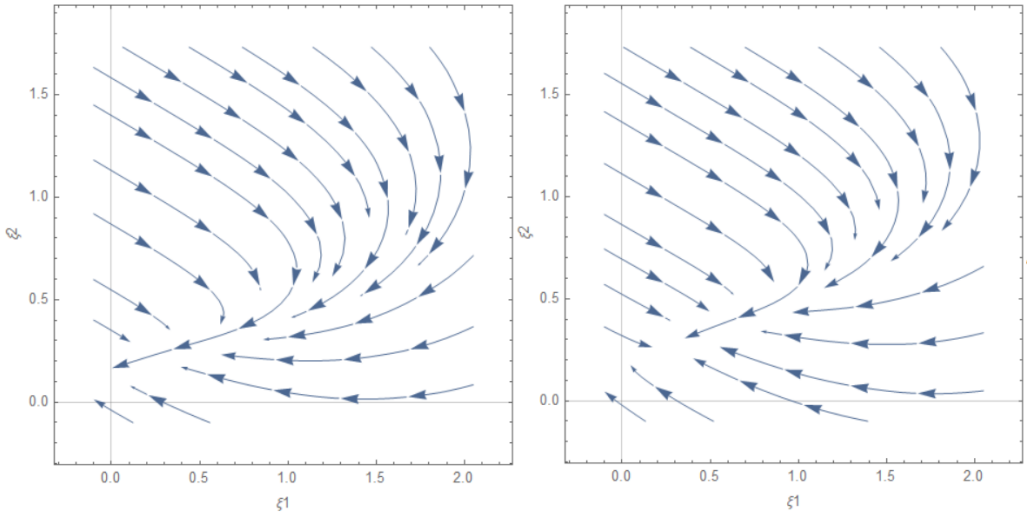

(a) Reference voltage on 9.5V

(b) Reference voltage on 13V

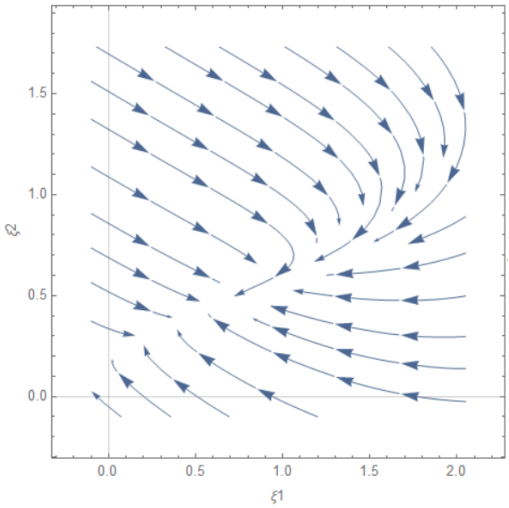

(c) Reference voltage on 16.5V

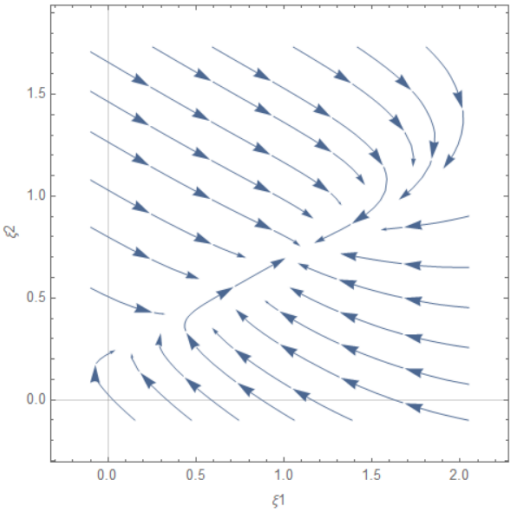

(d) Reference voltage on 20V

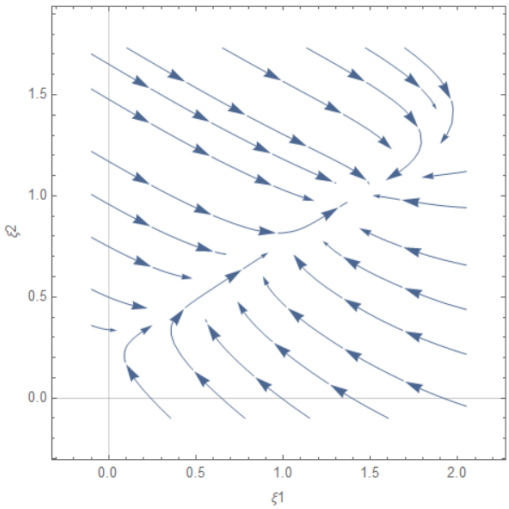

(e) Reference voltage on 23.5V

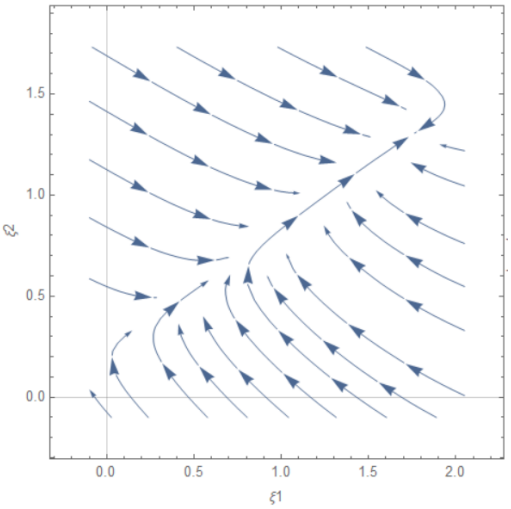

(f) Reference voltage on 27V

Figure 3.10: Proposed phase plane of the various reference points

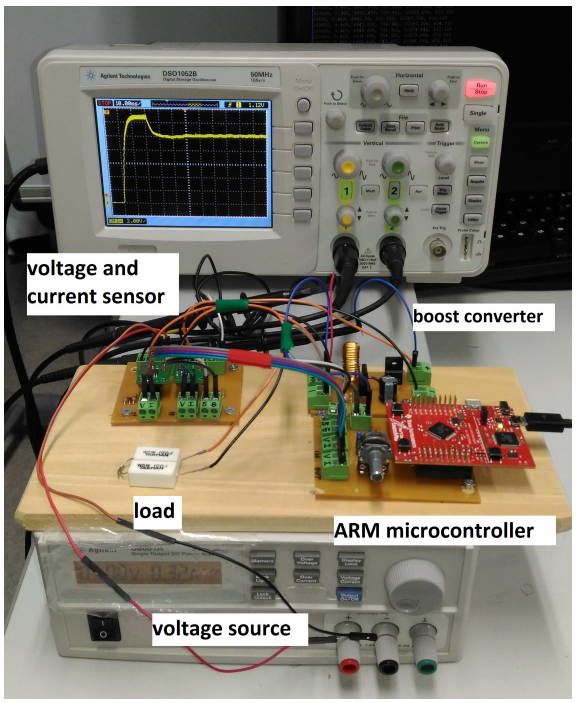

Figure 3.11: Experiment setup of nonlinear controller

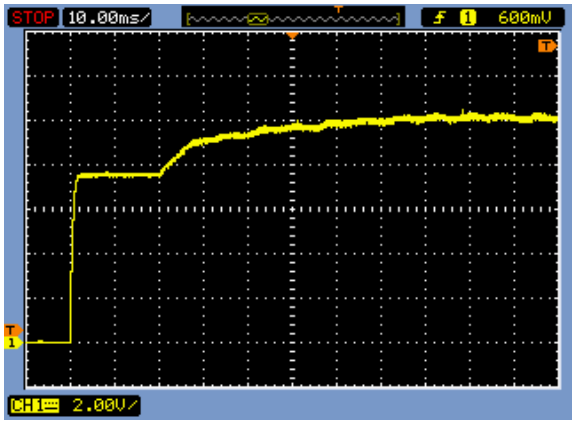

Figure 3.12: Output voltage measurement of Case-A

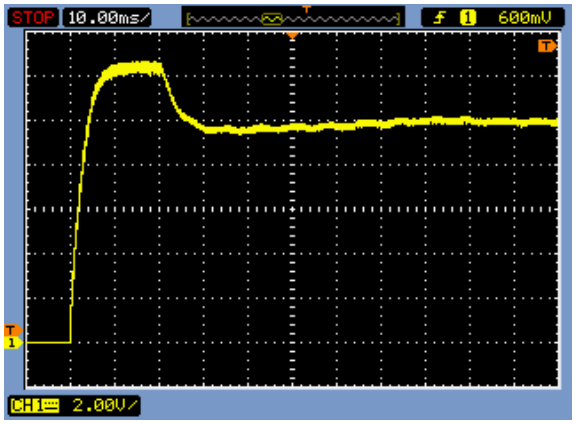

Figure 3.13: Output voltage measurement of Case-B

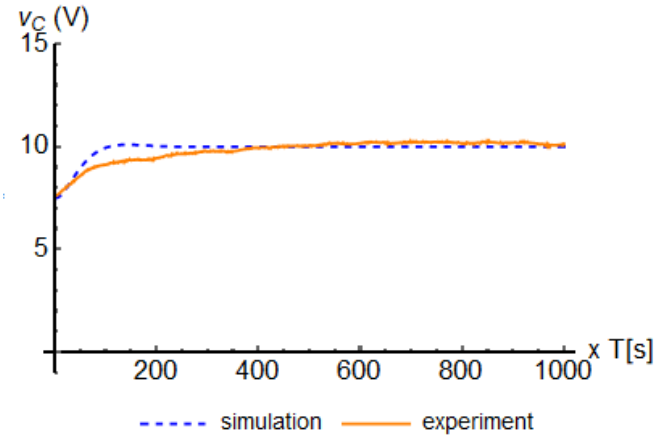

Figure 3.14: Output voltage comparison of Case-A

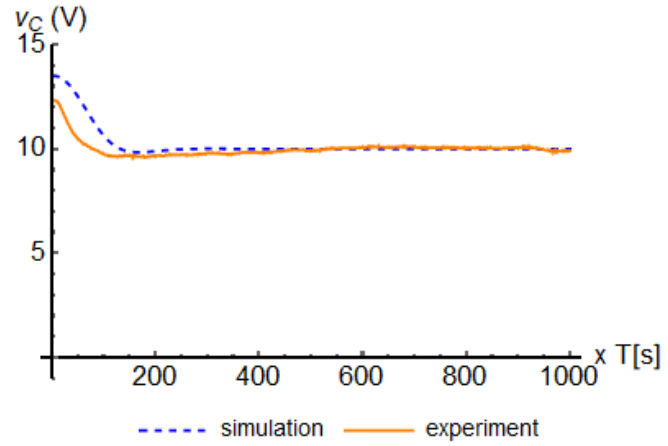

Figure 3.15: Output voltage comparison of Case-B

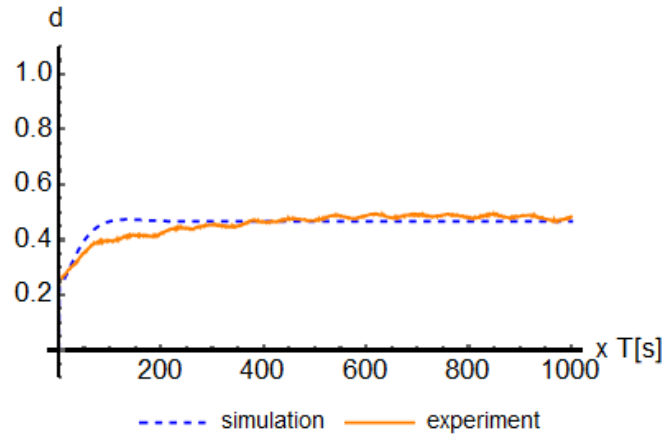

Figure 3.16: Duty-ratio comparison of Case-A

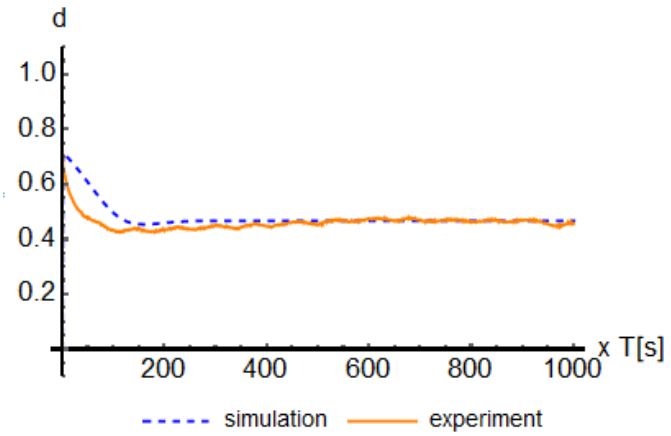

Figure 3.17: Duty-ratio comparison of Case-B

Chapter 4

Conclusion

The primary objective of this dissertation is to provide the solution of control problem in a power converter. The dissertation employs the model analysis, controller design and verification through simulation or experiment. The dissertation presents the novel steady-state model of the buck converter and novel nonlinear control of the boost converter.

The result of this study can be summarized as follows.

1. This dissertation shows that buck converter can be modeled in linear time-invariant (LTI) system so the various LTI control theory can be used to solve the problem on a buck converter. An accurate steady-state model is proposed to covers the shortage in describing the behavior of a buck converter in a steady state. The proposed model is presented in a summation of recovery function to describe the steady-state response accurately. The numerical circuit simulator checks the proposed steady-state model, and it shows the similar result with the proposed model.

2. The controller design using phase portrait can prevent the system to go beyond the designed mode. The phase portrait gives a visual trace of system response in several initial conditions and is useful in controller design. This study has proposed a novel nonlinear controller, and the controller guarantees boost converter always works in CCM for any initial condition. Moreover, the proposed controller can handle any reference point without retuning the parameters. The simulation result has shown that the proposed controller works well under different initial conditions. The experiment shows that the proposed nonlinear controller is implementable in hardware. The experiment result shows a good agreement with the simulation result.

For the future works, the author recommends applying the technique to the power system such as a photovoltaic system, hydrogen generator system, and the

others. The controller design technique also works to the other topologies of the power converter. The analysis on another load type such as a combination of resistive, inductive and capacitive load can be the next challenge in this research

References

[1] R.W. Erickson and D. Maksimovic. *Fundamental of Power Electronics*. Massachusetts, USA: Kluwer Academic Publisher, 2001.

[2] Muhammad H. Rashid. *Power Electronics Devices, Circuits, and Applications*. Essex, England: Pearson Education Limited, 2014.

[3] Christophe Basso. *Designing Control Loops for Linear and Switching Power Supplies*. London, England: Artech House, 2001.

[4] Wiliam A. Wolovich. *Automatic Control System*. USA: Saunders College Publishing, 1994.

[5] Eko Setiawan, Takuya Hirata, and Ichijo Hodaka. "Accurate Symbolic Steady State Modeling of Buck Converter". In: *International Journal of Electrical and Computer Engineering* 7.5 (2017), pp. 2374–2381. DOI: 10.11591/ijece.v7i5.pp2374-2381.

[6] Eko Setiawan and Ichijo Hodaka. "A Novel Nonlinear Control of Boost Converter using CCM Phase Plane". In: *International Journal of Electrical and Computer Engineering* 8.6 (2018).

[7] R. Middlebrook and S. Ćuk, eds. *A general unified approach to modelling switching-converter power stages* (Cleverand, USA). IEEE, June 1976. DOI: 10.1109/PESC.1976.7072895.

[8] R. W. Erickson, S. Ćuk, and R. Middlebrook, eds. *Large Signal Modeling and Analysis of Switching Regulators* (Cambridge, USA). IEEE, June 1982. DOI: 10.1109/PESC.1982.7072414.

[9] V. Tran and M. Mahd. "Modeling and Analysis of Transformerless High Gain Buck-boost DC-DC Converters". In: *International Journal of Power Electronics and Drive System (IJPEDS)* 4.4 (2014), pp. 528–535. DOI: 10.11591/ijpeds.v4i4.6386.

[10] J.S. Renius A et al. "Modelling of Variable Frequency Synchronous Buck Converter". In: *International Journal of Power Electronics and Drive System (IJPEDS)* 5.2 (2014), pp. 237–243.

[11] P. Szczesniak. “A Comparison Between Two Average Modelling Techniques of AC-AC Power Converters”. In: *International Journal of Power Electronics and Drive System (IJPEDS)* 6.1 (2015), pp. 32–44. DOI: 10.11591/ijpeds.v6.i1.pp32-44.

[12] D. A. Fernandes S. R. Naidu. “Technique for Simulating the Steady-State Response of Power Electronic Converter”. In: *IET Power Electronics* 4.3 (2011), pp. 269–277. DOI: 10.1049/iet-pel.2009.0321.

[13] L. Iannelli, F. Vasca, and G. Angelone. “Computation of Steady-State Oscillations in Power Converter Through Complementary”. In: *IEEE Transactions on Circuits and SystemsI: Regular Papers* 58.6 (2011), pp. 1421–1432. DOI: 10.1109/TCSI.2010.2094390.

[14] G.T. Kostakis, S.N. Manias, and N.I. Margaris. “A Generalized Method for Calculating the RMS Values of Switching Power Converters”. In: *IEEE Transactions on Power Electronics* 15.4 (2000), pp. 616–625. DOI: 10.1109/63.849031.

[15] M. Daryaei, M. Ebrahimi, and S.A. Khajehoddin, eds. *Accurate Parametric Steady State Analysis and Design Tool for DC-DC Power Converters* (Long Beach, USA). IEEE, Mar. 2016. DOI: 10.1109/APEC.2016.7468228.

[16] H.M. Mahery and E. Babaei. “Mathematical Modeling of Buck-boost DC-DC Converter and Investigation of Converter Element on Transient and Steady State Responses”. In: *International Journal of Electrical Power and Energy System* 44.1 (2013), pp. 949–963. DOI: 10.1016/j.ijepes.2012.08.035.

[17] B. Tsai, O. Trescases, and B. Francis, eds. *An Investigation of Steady-State Averaging for the Single-Inductor Dual Output Buck Converter using Fourier Analysis* (Boulder, USA). IEEE, June 2010. DOI: 10.1109/COMPEL.2010.5562362.

[18] R. Trinchero, I.S. Stievano, and F.G. Canavero. “Steady-State Analysis of Switching Power Converter via Augmented Time-Invariant Equivalents”. In: *IEEE Transaction on Power Electronics* 29.11 (2014), pp. 5657–5661. DOI: 10.1109/TPEL.2014.2322259.

[19] F. Misoc, M.M. Morcos, and J. Lookadoo, eds. *Fourier-Series Models of DC-DC Converters* (Carbondale, USA). IEEE, Sept. 2006. DOI: 10.1109/NAPS.2006.360144.

[20] R. Trinchero et al. “Steady-State Analysis of Switching Converter via Frequency-Domain Circuit Equivalents”. In: *IEEE Transactions on Circuits and SystemsII: Express Briefs* 63.8 (2016), pp. 748–752. DOI: 10.1109/TCSII.2016.2530299.

[21] G. Strang. *Computational Science and Engineering*. USA: Wellesley-Cambridge Press, 2007.

[22] S.D. Stallon, K.V. Kumar, and S.S. Kumar. "High Efficient Module of Boost Converter in PV Module". In: *International Journal of Electrical and Computer Engineering* 2.6 (2012), pp. 758–781. DOI: 10.11591/ijece.v2i6.1586.

[23] S. Bhat and H.N. Nagaraja. "Effect of Parasitic Elements on the Performance of Buck-Boost Converter for PV Systems". In: *International Journal of Electrical and Computer Engineering* 4.6 (2014), pp. 831–836. DOI: 10.11591/ijece.v4i6.6855.

[24] A. Boulahia, K. Nabti, and H. Benalla. "Direct Power Control for AC/DC/AC Converters in Doubly Fed Induction Generators Based Wind Turbine". In: *International Journal of Electrical and Computer Engineering* 2.3 (2012), pp. 425–432. DOI: 10.11591/ijece.v2i3.284.

[25] T.Z. Khaing and L.Z. Kyin. "Control Analysis of Stand-Alone Wind Power Supply System with Three Phase PWM Voltage Source Inverter and Boost Converter". In: *International Journal of Electrical and Computer Engineering* 5.4 (2015), pp. 798–809. DOI: 10.11591/ijece.v5i4.pp798-809.

[26] V. Ramesh and Y.K. Latha. "An Interleaved Boost Converter Based PFC Control Strategy for BLDC motor". In: *International Journal of Electrical and Computer Engineering* 5.5 (2015), pp. 957–966. DOI: 10.11591/ijece.v5i5.pp957-966.

[27] T. Raghu, S.C. Sekhar, and J.S. Rao. "SEPIC Converter based-Drive for Unipolar BLDC Motor". In: *International Journal of Electrical and Computer Engineering* 2.2 (2012), pp. 159–165. DOI: 10.11591/ijece.v2i2.306.

[28] M.Z. Hossain and N.A. Rahim. "Recent progress and development on power DC-DC converter topology, control, design and applications: A review". In: *Renewable and Sustainable Energy Reviews* 81.1 (2017), pp. 205–230. DOI: 10.1016/j.rser.2017.07.017.

[29] Z. Shen, N. Yen, and H. Min. "A Multimode Digitally Controlled Boost Converter with PID Autotuning and Constant Frequency/ Constant Off-time Hybrid PWM Control". In: *IEEE Transaction on Power Electronics* 26.9 (2011), pp. 2588–2598. DOI: 10.1109/TPEL.2011.2111464.

[30] L. Guo et al., eds. *Design of a digital control system for DC-DC converter to power electromagnets* (Lake Buena Vista, USA). IEEE, Oct. 2013. DOI: 10.1109/IAS.2013.6682495.

[31] M.M. Peretz and S. Ben-Yaakov. “Time-Domain Design of Digital Compensators for PWM DC-DC Converters”. In: *IEEE Transaction on Power Electronics* 27.1 (2011), pp. 284–293. DOI: 10.1109/TPEL.2011.2160358.

[32] S. Chander, P. Agarwal, and I. Gupta, eds. *FPGA-based PID Controller for DC-DC Converter* (New Delhi, India). IEEE, Dec. 2010. DOI: 10.1109/PEDES.2010.5712454.

[33] Y.I. Son and I.H. Kim. “Complementary PID Controller to Passivity-Based Nonlinear Control of Boost Converters With Inductor Resistance”. In: *IEEE Transactions on Control Systems Technology* 20.3 (2012), pp. 826–834. DOI: 10.1109/TCST.2011.2134099.

[34] O. Ibrahim, N.Z. Yahaya, and N. Saad, eds. *Comparative studies of PID controller tuning methods on a DC-DC boost converter* (Kuala Lumpur, Malaysia). IEEE, Aug. 2016. DOI: 10.1109/ICIAS.2016.7824044.